PLOS ONE

RESEARCH ARTICLE

Staurosporine and NEM mainly impair WNK-SPAK/OSR1 mediated phosphorylation of KCC2 and NKCC1

Jinwei Zhang[1,2], Antje Cordshagen[3], Igor Medina[4], Hans Gerd Nothwang[3,5,6], Jacek R. Wisniewski[7], Michael Winklhofer[5,8], Anna-Maria Hartmann[3,5]*

1 Hatherly Laboratories, Medical School, College of Medicine and Health, Institute of Biomedical and Clinical Sciences, University of Exeter, Exeter, United Kingdom, **2** Xiamen Cardiovascular Hospital, School of Medicine, Xiamen University, Xiamen, China, **3** Division of Neurogenetics, School of Medicine and Health Sciences, Carl von Ossietzky University Oldenburg, Oldenburg, Germany, **4** INSERM (Institut National de la Santé et de la Recherche Médicale) Unité 1249, INMED (Institut de Neurobiologie de la Méditerranée), Aix-Marseille University UMR 1249, Marseille, France, **5** Research Center for Neurosensory Sciences, Carl von Ossietzky University Oldenburg, Oldenburg, Germany, **6** Center of Excellence Hearing4all, Carl von Ossietzky University Oldenburg, Oldenburg, Germany, **7** Department of Proteomics and Signal Transduction, Biochemical Proteomics Group, Max-Planck-Institute of Biochemistry, Martinsried, Germany, **8** Institute for Biology and Environmental Sciences IBU, Carl von Ossietzky University of Oldenburg, Oldenburg, Germany

* anna.maria.hartmann@uol.de

OPEN ACCESS

Citation: Zhang J, Cordshagen A, Medina I, Nothwang HG, Wisniewski JR, Winklhofer M, et al. (2020) Staurosporine and NEM mainly impair WNK-SPAK/OSR1 mediated phosphorylation of KCC2 and NKCC1. PLoS ONE 15(5): e0232967. https://doi.org/10.1371/journal.pone.0232967

Editor: Jean-Claude Dussaule, Hopital Tenon, FRANCE

Received: November 26, 2019

Accepted: April 24, 2020

Published: May 15, 2020

Data Availability Statement: All relevant data are within the manuscript and its Supporting Information files.

Funding: This work was supported by the Deutsche Forschungsgemeinschaft (grants NO428/14-1 to H.G.N; and HA 6338/2-1 to A.-M. H). The work was further funded by Max-Planck Society for the Advancement of Science by the German Research Foundation (DFG/Gottfried Wilhelm Leibniz Prize to J.R.W.) and the National Natural Science Foundation of China (No.

Abstract

The pivotal role of KCC2 and NKCC1 in development and maintenance of fast inhibitory neurotransmission and their implication in severe human diseases arouse interest in post-transcriptional regulatory mechanisms such as (de)phosphorylation. Staurosporine (broad kinase inhibitor) and N-ethylmalemide (NEM) that modulate kinase and phosphatase activities enhance KCC2 and decrease NKCC1 activity. Here, we investigated the regulatory mechanism for this reciprocal regulation by mass spectrometry and immunoblot analyses using phospho-specific antibodies. Our analyses revealed that application of staurosporine or NEM dephosphorylates Thr^{1007} of KCC2, and Thr^{203}, Thr^{207} and Thr^{212} of NKCC1. Dephosphorylation of Thr^{1007} of KCC2, and Thr^{207} and Thr^{212} of NKCC1 were previously demonstrated to activate KCC2 and to inactivate NKCC1. In addition, application of the two agents resulted in dephosphorylation of the T-loop and S-loop phosphorylation sites Thr^{233} and Ser^{373} of SPAK, a critical kinase in the WNK-SPAK/OSR1 signaling module mediating phosphorylation of KCC2 and NKCC1. Taken together, these results suggest that reciprocal regulation of KCC2 and NKCC1 via staurosporine and NEM is based on WNK-SPAK/OSR1 signaling. The key regulatory phospho-site Ser^{940} of KCC2 is not critically involved in the enhanced activation of KCC2 upon staurosporine and NEM treatment, as both agents have opposite effects on its phosphorylation status. Finally, NEM acts in a tissue-specific manner on Ser^{940}, as shown by comparative analysis in HEK293 cells and immature cultured hippocampal neurons. In summary, our analyses identified phospho-sites that are responsive to staurosporine or NEM application. This provides important information towards a better understanding of the cooperative interactions of different phospho-sites.

81970238 to J.Z.). The funders had no role in study design, data collection and analysis, decision to publish, or preparation of the manuscript.

Competing interests: The authors have declared that no competing interests exist.

Introduction

The cation chloride cotransporter family (CCCs) consists of electroneutral secondary active cotransporters that mediate the symport of cations (Na^+ and K^+) coupled with chloride ions (Cl^-) across the plasma membrane. CCCs are divided into K^+-Cl^- outward cotransporters (KCC1-4), Na^+, K^+, Cl^- inward cotransporters (NKCC1-2, NCCs), the polyamine transporter CCC9, and the CCC-interacting protein CIP1 [1–3]. These transporters play a crucial role in various physiological processes like regulation of cell volume, directional ion transport across epithelial cells, secretion of K^+, and regulation of intracellular Cl^-concentration ($[Cl^-]_i$) in neurons [2, 4–11].

In neurons, KCC2 and NKCC1 are involved in the development and maintenance of inhibitory neurotransmission. For instance, KCC2 generates a low $[Cl^-]_i$ required for fast inhibitory neurotransmission. Binding of γ-aminobutyric acid (GABA) or glycine to their receptors, which are ligand-gated Cl^- channels, leads to a Cl^- influx and therefore hyperpolarization [8, 12]. By contrast, NKCC1 is more prevalent in immature inhibitory neurons. There, its action results in a high $[Cl^-]_i$ causing GABA or glycine to elicit a depolarizing action that opens L-type voltage-gated Ca^{2+} channels necessary for proper synapse formation [13–18].

The physiological relevance of the two cotransporters is corroborated by the phenotypes present in knockout mice. Mice with disruption of the gene *Slc12*a5 encoding both KCC2 isoforms (KCC2a and KCC2b), die shortly after birth due to motor deficits [19, 20]. Furthermore, dysfunction of KCC2 is associated with neurological and psychiatric disorders including epilepsy, neuropathic pain, spasticity, ischemic insults, brain trauma, schizophrenia, and autism [21–32]. Mice with disruption of *Slc12*a2 (NKCC1) are viable, but suffer from peripheral deafness, postnatal hyperexcitability and anti-convulsant, pain perception and male infertility [33–36]. Inhibition of KCC2 promotes formation of pathological conditions whereas inhibition of NKCC1 seems to prevent or at least alleviate pathological phenotypes [37]. This renders these two transporters a prime pharmacotherapeutic target and fosters interest in understanding posttranslational mechanisms of their regulation [12, 38–40]. The main focus is set on phospho-related mechanisms. The broad kinase inhibitor staurosporine was used to enhance KCC2 transport activity in immature auditory brainstem [41] and hippocampal cultured neurons [42], and to decrease NKCC1 activity [43–46]. Furthermore, N-ethylmaleimide (NEM), that likely modulates the activity of kinases and phosphatases, activates KCC2 [47–50] and inhibits NKCC1 [45, 51]. Thus, both compounds reciprocally regulate KCC2 (activation) and NKCC1 (inhibition). Understanding their mode of action provides the basis for further pharmacological studies and important insight into the molecular mechanisms involved in physiological regulation of these two transporters.

Since KCC2 and NKCC1 are present in the same neuronal populations but transport K^+ and Cl^- in opposite direction [52–54], regulatory mechanisms are required to coordinate their activity [4, 38, 55–60]. Indeed, several kinases and phosphatases regulate their transport activity. *In vitro* and *in vivo* analyses revealed that members of the with-no-lysine kinase (WNKs) family in combination with their downstream targets STE20/SPS1-related proline/alanine rich kinase (SPAK) and oxidative stress response kinase (OSR1) are the most prominent kinases that regulate KCC2 and NKCC1 activity in a reciprocal way. SPAK/OSR1, activated by WNK1, phosphorylate Thr^6 and Thr^{1007} of KCC2 [48, 59, 61–64]. WNKs also interact with a yet unknown kinase to phosphorylate Thr^{906} of KCC2 [48, 63]. Site-directed mutagenesis studies indicate that simultaneous mutation of Thr^{906} and Thr^{1007} to alanine (mimicking the dephosphorylated state) activates KCC2 [61, 65–67]. WNK/SPAK/OSR1 also phosphorylates the N-terminal residues Thr^{203}, Thr^{207}, Thr^{212} and Thr^{217} of NKCC1 [38, 59, 60, 68–76]

thereby activating NKCC1 [72, 75]. Thus dephosphorylation (KCC2) and phosphorylation (NKCC1) of WNK/SPAK/OSR1 specific phospho-sites enhance KCC2 and NKCC1 activity.

Phosphorylation can also enhance KCC2 activity. Phosphorylation of Ser^{932}, Thr^{934}, Ser^{937}, or the protein kinase C (PKC) site Ser^{940}, all residing in exon 22, increases its transport activity [47, 68, 77]. The multiplicity of phosphorylation/dephosphorylation sites on KCC2 offers a complex toolbox to gradually fine-regulate its activity and integrate different signaling pathways [4, 40, 65, 68].

Initially, both staurosporine and NEM were thought to act through a similar mechanism [47], but recent findings revealed that they act differentially on specific KCC2 phospho-sites [40]. Furthermore, staurosporine and NEM mediated effects involve both KCC2 phosphorylation and dephosphorylation [40, 48]. To gain insight into their mode of action, we analyzed the impact of these compounds on phosphorylation of specific KCC2 and NKCC1 phospho-sites using large-scale phosphoproteomics studies and phospho-site specific antibodies in stably transfected HEK293 cells and immature primary cultures of hippocampal neurons.

Material and methods

Cell culturing of HEK293 cells

For K^+-Cl^- cotransporter activity measurements, stably transfected rat KCC2b HEK293 cells ($HEK^{rnKCC2b}$) [55] were plated in a 0.1 mg/ml poly-L-lysine coated black-well 96 well culture dish (Greiner Bio-One, Frickenhausen, Germany) at a concentration of 100,000 cells/well. The remaining cells were plated on a 0.1 mg/ml poly-L-lysine-coated class coverslip and ~18 h later analyzed by immunocytochemistry.

Primary cultures of rat hippocampal neuron

All animal procedures were carried out in accordance with the European Union Directive of 22 September (2010/63/EU). The protocol was approved by the INSERM Local committee (Number 0287.01, delivered by Ministère de l'Education et de la Recherche). Hippocampi from 18-day-old rat embryos were dissected and dissociated using trypsin (0.05%) and plated in 60-mm culture dishes at a density of 100,000 cells cm^{-2} in minimal essential medium (MEM) supplemented with 10% NU serum (BD Biosciences, Le Pont de Claix, France), 10 mM glucose, 1 mM sodium pyruvate, 2 mM glutamine, and 100 U ml^{-1} penicillin–streptomycin as previously described [78]. On day 7 of culture incubation, half of the medium was changed to MEM with 2% B27 supplement (Invitrogen). 24 h prior to plating, dishes were coated with poly-ethylenimine (5 μg/ml).

Immunocytochemistry

For immunocytochemistry, all steps were performed at room temperature. HEK293 cells grown on poly-L-lysine-coated coverslips were fixated for 10 min with 4% paraformaldehyde in 0.2 M phosphate buffer (PBS). After three washing steps in PBS, cells were incubated with blocking solution (2% bovine serum albumin, 10% goat serum in PBS) for 30 min. Primary antibody solution (anti-KCC2 N1-12; 1:1,000; Neuromab, Carlifornia, USA) was added in carrier solution (0.3% Triton X-100, 1% bovine serum albumin, 1% goat serum in PBS) for 1 h. After washing three times in PBS, the secondary antibody, which was conjugated to a fluorescent probe (Alexa Fluor 488 goat anti-mouse; 1:1,000; Thermo Fisher Scientific, Bremen, Germany) was incubated for 1 h. After three washes in PBS, cells were mounted onto glass slides with Mowiol (Roth, Karlsruhe, Germany) and DAPI (Roth; 1:1,000). Photomicrographs were

taken using Biozero BZ-8100E (Keyence, Neu-Isenburg Deutschland) fluorescence microscope (Leica, Wetzlar, Germany).

Determination of K^+-Cl^- cotransport

KCC2 transport activity was determined by Cl^-dependent uptake of Tl^+ in HEK293 cells as previously described [47, 79, 80]. To initiate the flux measurement, the medium in the 96-well culture dish was replaced by 80 μl preincubation buffer (100 mM N-methyl-D-glucamine-chloride, 5 mM HEPES, 5 mM KCl, 2 mM $CaCl_2$, 0.8 mM $MgSO_4$, 5 mM glucose, pH 7.4, 160 mmol / kg ± 2,04 mmol/kg) supplemented with 2 μM FlouZin-2 AM dye (Thermo Scientific, Bremen, Germany) plus 0.2% (wt/vol) Pluronic F-127 (Thermo Scientific, Bremen, Germany) and incubated for 48 min at room temperature. Cells were then washed 3 times with 80 μl preincubation buffer and incubated for 15 min with 80 μl preincubation buffer plus 0.1 mM ouabain to block Na^+/K^+ ATPase activity. Three technical and five biological replicates were performed for each construct. Afterwards, the 96-well plate was placed into a fluorometer (Fluoroskan Accent, Thermo Scientific, Bremen, Germany) and each well was injected with 40 μl 5 x Tl^+ stimulation buffer (12 mM Tl_2SO_4, 100 mM NMDG, 5 mM Hepes, 2 mM KCl, 2 mM $CaCl_2$, 0.8 mM $MgSO_4$, 5 mM glucose, pH 7.4; 175 mmol/kg ± 2 mmol/kg). Fluorescence was determined in a kinetic dependent manner (excitation 485 nm, emission 538 nm, 1 frame in 5 s in a 200 s time span) across the entire cell population in a single well. By using linear regression of the initial values of the slope of Tl^+-stimulated fluorescence increase, transport activity was calculated [79, 80].

To determine the dose-response profile, increasing concentration of staurosporine (8–80 μM) and NEM (25–3000 μM) were applied to the preincubation buffer 15 min prior flux measurement. This was done for three technical replicates and at least five independent measurements were performed.

Statistical analyses

The majority of data populations illustrated in Figs 1, 3 and 4 showed non-normal distributions (verified using Shapiro-Wilk normality test at 0.05 significance level). Therefore, a non-parametric test (Wilcoxon-Mann-Whitney rank sum test) was employed for the comparison between different groups of data. The resulting p-values were adjusted with the Bonferroni correction for multiple testing. Note that only p-values < 0.01 were considered to reduce the chances of false positives (type I errors). The sample size n always refers to the number of biological replicates (independent preparations). The activity of each independent preparation was determined as mean over three technical replicates. The average scatter within technical replicates was 3 times smaller than the scatter across biological replicates for a given treatment.

For dose-response analyses, we used the nls function from the stats package in R (version 3.5.1) to model the data points with the Hill-Langmuir equation,

$$y(x; \mathrm{ED}_{50}, n, y_{\mathrm{sat}}) = y_0 + y_{\mathrm{sat}} \frac{x^n}{ED_{50}{}^n + x^n}, \quad (1)$$

where y is the Tl^+ uptake of $HEK^{rnKCC2b}$ cells, y_0 is the Tl^+ independent-baseline activity (y_0 = 100%), y_{sat} is the maximum activity (equivalent to V_{max} in reaction rate equation) relative to baseline, x is the concentration of the agonist, n is the Hill coefficient, and ED_{50} is the agonist concentration that produces 50% of the saturation response. The 95% confidence intervals for the dose response curves were determined with the function NonlinearModelFit ["MeanPredictionBands"] in Wolfram Mathematica. For the boxplots, the box extends from the upper (Q1) to the lower (Q3) quartile. The line inside the box represents the median. The whiskers

extend to the outermost data point that falls within upper inner and lower inner Quartile fences [Q1+1.5(IQR)] and [Q3-1.5(IQR)], respectively, where IQR = Q1-Q3 is the interquartile range.

Treatment of stably transfected HEK^{rnKCC2b} cells and hippocampal neurons

For mass spectrometry and immunoblot analyses, stably transfected HEK^{rnKCC2b} cells [55] were grown in 75 cm^2 cell-culture flask. Cells were washed with 5 ml flux hypotonic preincubation buffer (100 mM N-methyl-D-glucamine-chloride, 5 mM HEPES, 5 mM KCl, 2 mM $CaCl_2$, 0.8 mM $MgSO_4$, 5 mM glucose, pH 7.4; 160 mmol/kg±2,04 mmol/kg) and then treated with or without 8 μM staurosporine or 1 mM NEM. Cells were centrifuged at 500 rpm for 3 min and the resulting pellets used for immunoblot analyses or mass spectrometry analyses.

For immunoblot analyses of immature (9 days *in vitro*, (DIV)) rat hippocampal neurons, half of the media from culture dishes containing neurons (2.5 ml from each dish) was collected to prepare samples including 16 μM staurosporine (from 10 mM stock solution in DMSO), 1 mM NEM (by direct dissolving of the NEM powder) or DMSO (vehicle, same volume as for staurosporine), respectively. The samples were distributed dropwise into the culture dishes that gave final concentration of 8 μM staurosporine or 0.5 mM NEM and cultures were incubated 15 min at 37 ˚C (5% CO_2). After incubation, neurons were rinsed twice with Hanks' Balanced Salt solution (HBSS, ThermoFisher Scientific) precooled to 4 ˚C. The rinsage solution was replaced with ice-cold HBSS containing a cocktail of protease and phosphatase inhibitors (ThermoFisher Scientific) and neurons rapidly scraped and centrifuged at 4 ˚C (10,000 g, 3 min). Pellets were frozen in liquid nitrogen and kept for future analyses at -80 ˚C.

Multi-Enzyme Digestion Filter Aided Sample preparation (MED FAS)

For mass spectrometry analyses, cell pellets of untreated, staurosporine or NEM treated HEK^{rnKCC2b} cells were lysed in 2% SDS in 0.1 M Tris-HCl, pH 8.0, containing 0.1 M DTT as described previously [81]. Total protein was determined using WF-assay in micro-titer plate format [82]. Aliquots of the cell lysate containing 1–2 mg were processed in Amicon Ultra 15 Ultracel 30k (Merck Millipore, Darmstadt) devices as described previously [83] with several modifications using the MED FASP method [84]. Briefly, SDS and other low molecular weight material were removed by centrifugation at 4,000 x *g* in 5 consecutive washes with UA buffer containing 8 M urea (ultrapure, Merck, Darmstadt) in 0.1 M Tris pH 8. Following two washes with 5 ml of 0.1M Tris-HCl, pH 8 (DB buffer), 20 μg of LysC (Wako, Neuss) in 0.5 mL of DB was added to the filter. Samples were digested overnight at 37 ˚C and peptides were collected by centrifugation. Next, the material retained in the filter was cleaved with 10 μg trypsin in 0.5 ml DB at 37 ˚C for 4 h and the peptides were eluted as previously. To increase the yield of peptides, filters were washed twice with 0.5 mL DB. Concentration of peptides was determined by WF-assay [82].

TiO_2-based enrichment of phosphopeptides

Phosphopeptides were enriched using TiO_2-beads [85] with several modifications [83]. Briefly, 25 mg of 'Titansphere TiO_2 10 μm' (GL Sciences, Inc., Japan) were suspended in 50 μl of 3% (m/v) dihydroxybenzoic acid in 80% (v/v) CH_3CN, 0.1% CF_3COOH and diluted 1:4 with water before use. Ten microliters of this slurry (1 mg beads) were added and samples incubated under continuous agitation for 20 min. The mass ratio of the beads and peptides was 3:1. Then, the titanium beads were sedimented by centrifugation at 5,000 x *g* for 1 min and the supernatants were collected and mixed with another portion of the beads and incubated as

above. The bead-pellets were resuspended in 150 μl of 30% (v/v) CH_3CN containing 3% (v/v) CF_3COOH and transferred to a 200 μl pipet tip plugged with one layer of glass microfiber filter GFA (Whatman). The beads were washed three times with 30% (v/v) CH_3CN, 3% CF_3COOH (v/v) solution and three times with 80% CH_3CN (v/v), 0.3% CF_3COOH (v/v) solution. Finally, the peptides were eluted from the beads with 100 μL of 40% CH_3CN (v/v) containing 15% NH_4OH (m/v) and were vacuum-concentrated to $\sim$4 μl.

Mass-spectrometric analysis

Analysis of peptide mixtures was conducted using a QExactive HF-X mass spectrometer (Thermo-Fisher Scientific, Palo Alto). Aliquots containing $<$1 μg of total peptide were chromatographed on a 50 cm column with 75 μm inner diameter packed C_{18} material. Peptide separation occurred at 300 nl/min for 95 min using an acetonitrile gradient of 5–30%. The temperature of the column oven was 55˚C. The mass spectrometer operated in data-dependent mode with survey scans acquired at a resolution of 60,000. Up to the top 15 most abundant isotope patterns with charge $\geq$ +2 from the survey scan (300–1650 m/z) were selected with an isolation window of 1.4 m/z and fragmented by HCD with normalized collision energies of 25. The maximum ion injection times for the survey scan and the MS/MS scans were 20 and 28 ms, respectively. The ion target value for MS1 and MS2 scan modes was set to 3×10^6 and 10^5, respectively. The dynamic exclusion was 30 s. The MS spectra were searched using MaxQuant software. A maximum of two missed cleavages was allowed. The maximum false peptide and protein discovery rate was specified as 0.01. The whole mass spectrometry analyses were performed in three technical and two biological replicas per treatment.

Immunoblot and phospho-antibody immunoprecipitation analyses

Lysate protein samples were subjected to immunoblot and immunoprecipitation as previously described [63]. Protein samples (40 μg) were boiled in sample buffer for 5 min, resolved by 7.5% sodium dodecyl sulfate polyacrylamide-gel electrophoresis and electrotransferred onto a polyvinylidene difluoride membrane. Membranes were incubated for 30 min with TBST (Tris-buffered saline, 0.05% Tween-20) containing 5% (w/v) skim milk. Blots were then washed six times with TBST and incubated for 1 h at room temperature with secondary HRP-conjugated antibodies diluted 5000-fold in 5% (w/v) skim milk in TBST. After repeating the washing steps, signals were detected with enhanced chemiluminescence reagent. Immunoblots were developed using ChemiDoc™ Imaging Systems (Bio-Rad, Feldkirchen). Figures were generated using Photoshop/Illustrator (Adobe). Band densities of bands were measured with ImageJ. Calculation of intensity ratios is based on (phospho-dimeric KCC2 + phospho-monomeric KCC2) / (total dimeric KCC2 + total monomeric KCC2), (total dimeric KCC2 + total monomeric KCC2)/β-actin or tubulin, SPAK $pThr^{233}$/SPAK, SPAK $pSer^{373}$/SPAK, SPAK/β-actin or tubulin, NKCC1 $pThr^{203,207,212}$/NKCC1, NKCC1/β-actin or tubulin, as reported previously [66]. Mann–Whitney U-test was used for comparison between 2 independent groups and Wilcoxon matched pairs test was employed to compare paired data (GraphPad Prism 7.0, San Diego, CA, USA).

For phospho-antibody immunoprecipitation, KCC isoforms were immunoprecipitated from indicated cell extracts. 2 mg of the indicated clarified cell extract was mixed with 15 μg of the indicated phospho-specific KCC antibody conjugated to 15 μl of protein-G–Sepharose, in the added presence of 20 μg of the dephosphorylated form of the phosphopeptide antigen, and incubated 2 hours at 4 ˚C with gentle shaking. Immunoprecipitates were washed three times with 1 ml of lysis buffer containing 0.15 M NaCl and twice with 1 ml of buffer A. Bound proteins were eluted with 1x LDS sample buffer.

Antibodies

The following antibodies were purchased from Division of Signal Transduction Therapy Unit at the University of Dundee: KCC2A phospho-Thr^{906} (SAYTYER(T)LMMEQRSRR [residues 975–989 of human KCC3A] corresponding to SAYTYEK(T)LVMEQRSQI [residues 899–915 of human KCC2A], S959C); KCC2A phospho-Thr^{1007} (CYQEKVHM(T) WTKDKYM [residues 1032–1046 of human KCC3A] corresponding to TDPEKVHL(T) WTKDKSVA [residues 998–1014 of human KCC2A], S961C); SPAK/OSR1 (T-loop) phospho-Thr^{233}/Thr^{185} antibody (226–238 of human SPAK or residues 178–190 of human OSR1, TRNKVRKpTFVGTP, S204C); SPAK/OSR1 (S-motif) phospho-Ser^{373}/Ser^{325} antibody (367–379 of human SPAK, RRVPGSpSGHLHKT, which is highly similar to residues 319–331 of human OSR1 in which the sequence is RRVPGSpSGRLHKT, S670B); SPAK (427–443 of human SPAK, QSLSVHDSQGPPVGTP, S849C); NKCC1 phospho-Thr203+Thr207+Thr212 (residues 198–217 of human NKCC1, HYYYDpTHTNpTYYLRpTFGHNT, S763B); NKCC1 phospho-Thr^{212}/Thr^{217} (residues 208–223 of human NKCC1, YYLRpTFGHNpTMDAVPR, S063D); NKCC1-total antibody (residues 1–260 of shark NKCC1, S841B). Pan-KCC2 antibody (residues 932–1043 of human KCC2) was from NeuroMab (73–013). KCC2 phospho-Ser940 antibody was from ThermoFisher Scientific (PA5-95678). PKCδ phospho-Thr^{505} antibody (9374) and β-Actin (D6A8) antibody (12620) were from Cell Signaling Technology. Anti (neuronal)-β-Tubulin III antibody was from Sigma-Aldrich (T8578). Secondary antibodies coupled to horseradish peroxidase used for immunoblotting were obtained from Pierce. IgG used in control immunoprecipitation experiments was affinity-purified from pre-immune serum using Protein G-Sepharose.

Results

Dose-response analyses of staurosporine and NEM in stably transfected HEK^{rnKCC2b} cells

Staurosporine and NEM generally activate KCCs [40, 47, 86, 87]. To closer characterize their mode of action, we used stably transfected HEK^{rnKCC2b} cells, as high amount of the cotransporter is advantageous for subsequent biochemical analyses. Immunoreactivity of HEK^{rnKCC2b} cells against KCC2 was detected in all cells with clear labeling at the cell membrane and cytosol (Fig 1A). This is in agreement with previous cell surface expression analyses that detected 11.8 ± 1.4% of total KCC2 in stably transfected *rn*KCC2b at the cell surface [79].

To quantify the impact of staurosporine and NEM on *rn*KCC2b transport activity, Tl^+ flux measurements were performed [79, 80, 88]. Transport activity in HEK^{rnKCC2b} cells was 5.6 times higher compared to background (HEK^{rnKCC2b} 100% ± 5.32%; mock; 17.7% ± 5.5%; $p = 4.3x10^{-5}$; n = 5) (Fig 1B). Here and elsewhere in the text, numbers indicate mean +/- SD, *p* was determined using Wilcoxon-Mann-Whitney rank sum test. Treatment with 10 μM staurosporine or 1 mM NEM resulted in an approximately twofold increase of *rn*KCC2b activity compared to untreated HEK^{rnKCC2b} cells (staurosporine: 187.5% ± 37.1%, $p = 3x10^{-3}$; NEM: 204% ± 23.2%; $p = 3x10^{-3}$). The loop diuretics furosemide, that specifically inhibits the function of cation chloride cotransporters [89, 90], significantly inhibited the function of *rn*KCC2b (34.7 ± 12.2%, $p = 4\ x10^{-5}$).

Next, we determined the dose-response relationships of staurosporine and NEM on *rn*KCC2b transport activity by treating HEK^{rnKCC2b} cells with different concentrations of staurosporine (5–80 μM) or NEM (25–3,000 μM). Fig 2 represents the dose-response curve for both agents. The dose-response curve for staurosporine (Fig 2A) was approximately a rectangular hyperbola ($n \approx 1$, not significantly different from unity). This reflects Michaelis-Menten

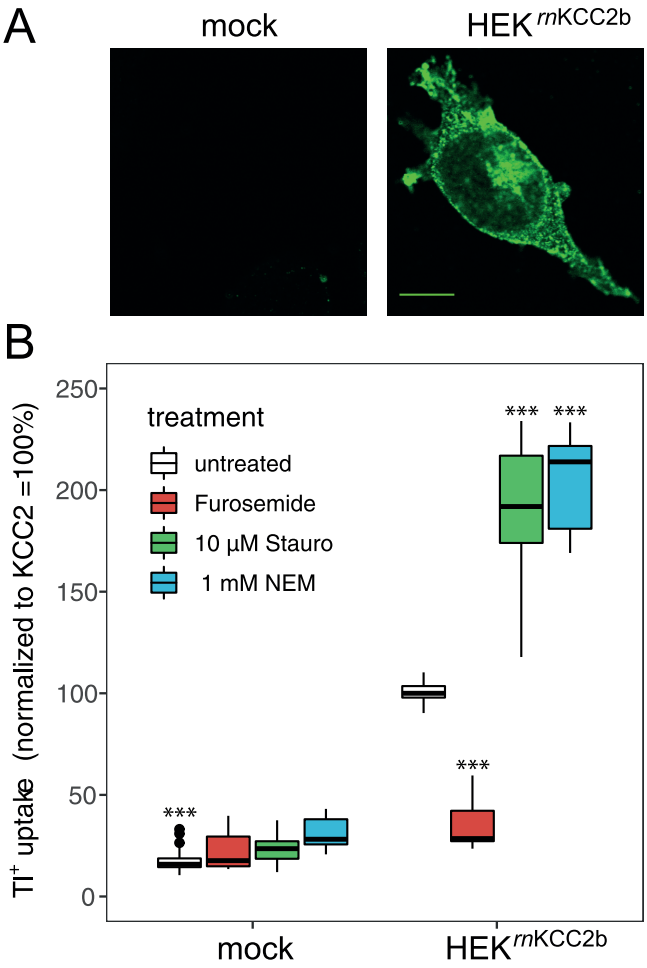

Fig 1. Staurosporine and NEM increase KCC2 activity. A: Immunoreactivity of stably transfected HEK^{rnKCC2b} cells was detected with labeling at the cell membrane and cytosol. Photomicrographs were taken with a confocal laser-scanning microscope. Scale bar, 10 μm. B: Transport activity of *rn*KCC2b was determined by Tl^+ flux measurements. Treatment with 10 μM staurosporine or 1 mM NEM resulted in an approximately twofold increase of *rn*KCC2b activity. Application of the loop diuretics furosemide (2 mM) significantly inhibited *rn*KCC2b function. The graph represents the data of at least five independent measurements (each consisting of three technical replicates) normalized to *rn*KCC2b. Statistical analyses: ***, $p < 0.001$ versus HEK^{rnKCC2b}; Error bars represent SD.

https://doi.org/10.1371/journal.pone.0232967.g001

kinetics and suggests absence of cooperative effects. In contrast, the dose response curve for NEM (Fig 2B) had a pronounced sigmoidal shape ($n \approx 5$), which reflects cooperative binding kinetics. The effective dose ED_{50} (representing the potency) for staurosporine of stably transfected HEK^{rnKCC2b} was 12.8 ± 4.9 μM and the maximal efficacy (E_{max}) was 205 ± 40%. The ED_{50} value for NEM was 0.5 ± 1.3 mM and E_{max} was 105 ± 6%. For further analyses, we used a concentration of 8 μM staurosporine and 1 mM NEM, if not indicated otherwise as these concentrations significantly increase KCC2b transport activity.

Identification of CCC phosphorylation sites in stably transfected HEK^{rnKCC2b} cells by mass spectrometry analyses upon treatment with staurosporine or NEM

Phosphoproteomics by mass spectrometry has the advantage of providing an unbiased survey of phospho-sites. Therefore, we here used for the first time this technique to gain insight on

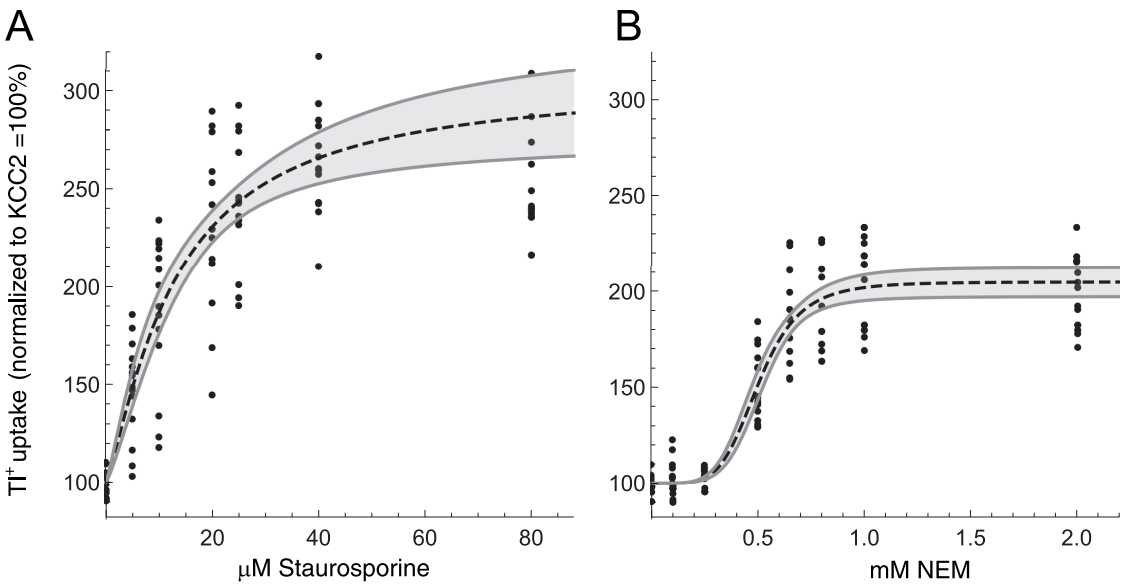

Fig 2. Dose-response relationship of staurosporine and NEM on KCC2 transport activity. HEK$^{rn\text{KCC2b}}$ cells were treated with different concentrations of staurosporine (5–80 μM; A) or NEM (25–3,000 μM; B) for 15 min. Transport activity of *rn*KCC2b was determined by Tl^+ flux measurements. Treatment with staurosporine resulted in a classical Michaelis-Menden curve, whereas NEM treatment showed a sigmoidal curve with a Hill coefficient of 5.2 ± 1.3 indicating a positive cooperative effect on *rn*KCC2b. The graph represents the data of at least five independent measurements (each consisting of three technical replicates) normalized to untreated HEK$^{rn\text{KCC2b}}$.

https://doi.org/10.1371/journal.pone.0232967.g002

the impact of staurosporine and NEM on *rn*KCC2b phospho-sites in HEK$^{rn\text{KCC2b}}$. For each condition, two biological and three technical replicas were performed. Phospho-sites detected in at least one technical experiment are listed in Table 1. We first mapped KCC2b phospho-sites in untreated HEK$^{rn\text{KCC2b}}$ cells. Twelve phospho-sites were identified: Ser^{25}, Ser^{26}, Ser^{31}, Thr^{32}, Thr^{34} in the cytoplasmic N-terminus and Thr^{906}, Ser^{937}, Ser^{940}, Thr^{1007}, Ser^{1022}, Ser^{1025}, and Ser^{1026} in the C-terminus (Table 1, untreated). These sites include all phospho-sites already present in PhosphositePlus (Table 2) [91]. Recently phosphoproteomic data deposited in Phosida and Phosphosite plus revealed that rat KCC2b tissue only harbors seven phospho-sites (Table 2). Thus, we here report five phospho-sites (Ser^{25}, Thr^{32}, Thr^{906}, Ser^{937} and Thr^{1007}) that were so far only reported for mouse but not rat KCC2 tissue (Table 2). These sites most likely reflect different expression of kinases and phosphatases in different tissues (HEK293 vs. rat brain tissue) [69] or increased detection rate in stably transfected HEK$^{rn\text{KCC2b}}$ cells.

As KCC1, KCC4, and NKCC1 are endogenously expressed in HEK293 cells and as mass spectrometric analysis provides data on most proteins in a given sample, we also investigated phosphorylation sites of the following proteins: *hs*KCC1 (Thr^{893}, analogous to *rn*KCC2b Thr^{1007}), *hs*KCC4 (Thr^{926} and Thr^{980}, analogous to *rn*KCC2b Thr^{906} and Thr^{1007}) and *hs*NKCC1 (Thr^{212}, Thr^{217}, Ser^{242}, Thr^{266}, Thr^{268}, Ser^{940}, Tyr^{956}, and Ser^{957}). These phospho-sites were already previously deposited in PhosphositePlus and Phosida (S1–S3 Tables). Overall, we detected only a low proportion of all so far deposited phospho-sites for these three cotransporters. This might reflect low expression levels in HEK293 cells.

Next, we investigated the phosphorylation pattern of *rn*KCC2b upon staurosporine and NEM treatment. Phosphorylation at Ser^{26}, Thr^{32}, Thr^{34}, Thr^{906}, Ser^{940}, Thr^{1007}, Ser^{1022}, Ser^{1025}, Ser^{1026} of *rn*KCC2b were still present upon treatment with staurosporine or NEM, whereas

Table 1. Phospho-sites of stably transfected HEK^{rnKCC2b} cells. Stably transfected HEK^{rnKCC2b} were treated with or without 1 mM NEM or 8 μM staurosporine before they were analyzed by mass spectrometry. The protein accession numbers are: *hs*NKCC1 (P55011), *hs*KCC1 (Q9UP95), *rn*KCC2b (Q9H2X9-2), *hs*KCC4 (Q9Y666).

Sample	Phosphorylation sites	Phosphopeptides	untreated	NEM treated	staurosporine treated
***hs*NKCC1**	T212; T217	**T**FGHN**T**MDAVPR	(2)		
	S242	LLRP**S**LAELHDELEK	(1)	(1)	
	T266	EPFEDGFANGEES**T**PTR	(3)	(2)	(2)
	S940	EGLDISHLQGQEELLS**S**QEK	(2) (2)	(2) (1)	(3) (1)
	Y956; S957	DVVVSVE**YS**KK	(3) (2)	(3) (1)	(3) (3)
***hs*KCC1**	T983	IQM**T**WTRDK	(2)		
***rn*KCC2b**	S25; S26	E**SS**PFINSTDTEK	(1)		
	S26	ES**S**PFINSTDTEK	(2) (3)	(3) (3)	(3) (3)
	S31	ESSPFIN**S**TDTEK	(2)	(1)(1)	
	T32	ESSPFINS**T**DTEK	(1)	(1)	(1)
	T34	ESSPFINSTD**T**EK	(3) (2)	(2)	(1)
	T906	**T**LVMEQRSQILK	(3)	(3)	(3)
	S937	EIQSITDE**S**RGSIR	(2)		
	S940	EIQSITDESRG**S**IR	(2) (3)	(2)	(1)
	T1007	VHL**T**WTK	(3)	(3)	(3)
	S1022; S1025	GP**S**PV**S**SEGIK	(3) (1)	(3)	(3) (1)
	S1022; S1025; S1026	GP**S**PV**SS**EGIK	(1)	(1)	
	S1022; S1026	GP**S**PVS**S**EGIK	(3)	(3)	(3)
	S1026	GPSPVS**S**EGIK	(3)	(3)	(3)
***hs*KCC4**	T926	**T**LMMEQR	(2)		
	T980	VQM**T**WTREK	(3)	(1)	

The number in brackets indicates in how many technical replica a given phospho-site was detected (max. 3). Each bracket provides the results of one biological experiment.

https://doi.org/10.1371/journal.pone.0232967.t001

phosphorylation of Ser^{25} and Ser^{937} was not detected anymore in either of the two conditions (Table 1). Additionally, no phosphorylation was detected for Ser^{31} after treatment with staurosporine.

Regarding endogenously expressed CCCs, the phospho-site Thr^{983} of *hs*KCC1 (analogous to *rn*KCC2b Thr^{1007}), Thr^{926} of *hs*KCC4 (analogous to *rn*KCC2b Thr^{906}) and Thr$^{212/217}$ and Thr$^{266/268}$ of *hs*NKCC1 could not be detected upon application of either of the two reagents. Additionally, the phospho-sites Thr^{980} of *hs*KCC4 (analogous to *rn*KCC2b Thr^{906}) and Ser^{242} of *hs*NKCC1 were not detected anymore after staurosporine treatment. The phospho-sites Thr^{266}, Ser^{940} and Tyr^{956}/Ser^{957} of *hs*NKCC1 were still present upon treatment with staurosporine and NEM.

Several kinases were described to directly phosphorylate KCC2 and NKCC1. This includes kinases of the WNK-SPAK/OSR1 and PKC mediated phosphorylation pathways. To gain further insight into the regulatory phosphorylation mechanism, we explored their phosphorylation pattern as well. We detected several phosphorylation sites in *hs*WNK1, *hs*WNK2, and *hs*SPAK [69, 93, 94] (Table 3). Upon all, we observed phosphorylation of the activating T-loop residue Ser^{382} of *hs*WNK1 and the S-loop phosphorylation site of Ser$^{372/373}$ of *hs*SPAK that is phosphorylated by WNK1 [63, 69, 93]. Upon treatment with staurosporine or NEM, Ser^{382} of *hs*WNK1 and Ser$^{372/373}$ of *hs*SPAK were not detected anymore (Table 4). We were not able to detect phosphorylation of Thr^{233} that is located in the T-loop kinase domain of *hs*SPAK. Normally, this site is directly phosphorylated by WNK1 and WNK4 to activate SPAK [60, 63, 69,

Table 2. Phospho-sites in PhosphoSitePlus and PHOSIDA detected by mass spectrometry analyses.

Phosphosite Plus *rn*KCC2b	Phosphosite Plus *hs*KCC2b	Phosphosite Plus *mm*KCC2b	Phosida *mm*KCC2b	Transport activity measured by:
-	-	**S^{25}**	**S^{25}**	[47, 65]
S^{26}	-	**S^{26}**	**S^{26}**	[47, 65]
S^{31}	**S^{31}**	-	**S^{31}**	(40)
-	-	-	**(T^{32})**	-
T^{34}	**T^{34}**	**T^{34}**	**T^{34}**	[40, 92]
-	Y^{594}	-	-	-
-	S^{599}	-	-	-
-	-	-	S^{649}	-
-	T^{798}	-	-	-
-	T^{808}	-	-	-
-	-	**T^{906}**	**T^{906}**	[47, 61, 66]
-	-	S^{913}	-	-
-	-	S^{932}	(S^{932})	[40]
-	-	-	(T^{934})	[47]
-	-	**S^{937}**	**S^{937}**	[47]
S^{940}	-	**S^{940}**	**S^{940}**	[48, 77]
-	-	S^{988}	-	-
-	-	T^{999}	-	[40]
-	-	**T^{1006}**	**T^{1006}**	[47, 48, 61, 66]
-	-	-	T^{1008}	[40]
S^{1022}	-	**S^{1021}**	**S^{1021}**	[47]
S^{1025}	-	**S^{1024}**	**(S^{1024})**	[47]
S^{1026}	-	**S^{1025}**	**S^{1025}**	[47]
-	-	S^{1044}	-	-

Abbreviations used are as follows: *rn*, *Rattus norvegicus*; *hs*, *Homo sapiens*; *mm*, *Mus musculus*. Phospho-sites detected in the present mass spectrometry study are marked in bold.

https://doi.org/10.1371/journal.pone.0232967.t002

95]. Furthermore, we did not detect any phospho-sites of the ubiquitously expressed WNK3 and WNK4. Again, this probably results from low expression rates in HEK293 cells.

PKC mediates the phosphorylation of KCC2 and NKCC1 [48, 77, 96, 97]. The PKC family consists of 10–12 isoforms grouped into three classes [98–101]. We detected several phospho-sites in seven *hs*PKC family members (alpha, beta, delta, epsilon, theta, eta and iota; Table 4).

To summarize, according to mass spectrometry based phosphoproteome analyses, staurosporine and NEM reduce the number of detected phospho-sites of stably expressed *rn*KCC2b and endogenously expressed *hs*KCC1, *hs*KCC4, *hs*NKCC1, *hs*WNK1 and *hs*SPAK. Phosphorylation of some sites (*rn*KCC2b: Ser^{31}, *hs*NKCC1:Ser^{242}, *hs*KCC4: Thr^{980}) was absent only after staurosporine treatment. Yet, these results can only be used as an indication since the absence of phosphorylation sites can reflect detection problems caused by low phosphorylation rates.

Quantitative analyses of phospho-sites of *rn*KCC2b and *hs*NKCC1 upon staurosporine and NEM treatment in HEK$^{rn\text{KCC2b}}$ cells

The experimental setup of our mass spectrometry-based analysis precluded quantification of changes at individual phospho-sites. We therefore applied in a next step phospho-site-specific antibody, as they were previously shown to quantitatively monitor changes in KCC2, NKCC1 and SPAK phosphorylation [23, 48, 59, 66, 70, 102]. Currently, a limited number of this class

Table 3. Phospho-sites of *hs*SPAK, *hs*WNK1 and *hs*WNK2 endogenously expressed in stably transfected HEK^{rnKCC2b} cells. Stably transfected HEK^{rnKCC2b} were treated with or without 1 mM NEM or 8 μM staurosporine before they were analyzed by mass spectrometry. The protein accession numbers are: *hs*SPAK (AAC72238.1), *hs*WNK1 (Q9H4A3.2), *hsWNK2* (Q9Y3S1.4).

sample	Phosphorylation site	Phosphopeptides	untreated	staurosporine treated	NEM treated
***hs*SPAK**	308	EMMKK**Y**GK	(2) (1)	(1)	(2)
	354	LL**T**RTPDIAQRAK	(1)	(2)	(1)
	356	LLTR**T**PDIAQRAK	(2)	(2)	(1)
	403	AAF**S**QEK	(3)	(1)	(1)
	518; 520	ALK**T**L**T**FK	(3) (2)	(2) (3)	(3) (3)
	372; 373	VRRVPG**SS**GHLHK	(1)		
***hs*WNK1**	11	QS**S**TPGSLFLSPPAPAPK	(2)	(1)	
	167; 170	DRPV**S**QP**S**LVGSK	(3)	(2)	(3)
	167; 174	DRPV**S**QPSLVG**S**K	(3)	(3)	(2)
	170	DRPVSQP**S**LVGSK	(3)		(2)
	174	DRPVSQPSLVG**S**K	(3) (3)	(3) (3)	(2) (3)
	183	EEPPPAR**S**GSGGGSAK		(1)	(1)
	185	EEPPPARSG**S**GGGSAK		(1)	
	183; 185	EEPPPAR**S**G**S**GGGSAK	(3)	(3)	(3)
	382	**S**VIGTPEFMAPEMYEEK	(1)		
	599	QQVEQSSA**S**QTGIK	(2) (3)	(3) (3)	(2)
	1220	DDYGFSG**S**QK	(2)	(1)	
	1849	EGPVLAT**S**SGAGVFK	(3)	(1)	
	1978	EGPVA**S**PPFMDLEQAVLPAVIPK	(3)	(3)	(3)
	2121	VPPAVIIPPAAPL**S**GR	(2)		(1)
	2245	G**T**FTDDLHK	(1)		
	2372	SI**S**NPPGSNLRTT	(3) (3)	(3) (3)	(3)
***hs*WNK2**	560	EQQDVG**S**PDK	(2)	(3)	(3)
	1889	AG**S**LGPETPSR	(3)	(3)	(3)
	1862	QA**S**LPVSGSVAGDFVK	(1) (3)		(2) (1)

The number in brackets indicates in how many technical replica a given phospho-site was detected (max. 3). Each bracket provides the results of one biological experiment.

https://doi.org/10.1371/journal.pone.0232967.t003

of antibodies is available for CCCs. They are directed against the well-known phospho-sites Ser^{940}, Thr^{906} and Thr^{1007} in *rn*KCC2b and Thr$^{203,\ 207,\ 212}$ in *hs*NKCC1. So far, no data are available for the staurosporine and NEM effect on Thr^{906} in *rn*KCC2b and Thr$^{203,\ 207,\ 212}$ in *hs*NKCC1 and the staurosporine effect on Ser^{940}, and Thr^{1007} in *rn*KCC2b. To examine the impact of staurosporine and NEM on the phosphorylation level of these sites, we treated HEK^{rnKCC2} cells with 8 μM staurosporine, 1 mM NEM or DMSO as a vehicle control for 15 min. Lysates were probed for KCC2 or NKCC1 and phosphorylation levels of each phospho-site were quantified (Fig 3). As previously described, positions Ser^{940}, Thr^{906} and Thr^{1007} are phosphorylated in KCC2b, and Thr$^{203,\ 207,\ 212}$ in NKCC1 of untreated HEK^{rnKCC2} cells [48, 70, 102] (Fig 3). These data corroborate the phosphoproteome analyses which revealed phosphorylation of Ser^{940}, Thr^{906} and Thr^{1007} in KCC2b and Thr^{212}/Thr^{217} in NKCC1 as well (Table 1).

Next, we observed the impact of staurosporine and NEM on these phospho-sites (Fig 3). Both agents decreased the phosphorylation status of the WNK/SPAK sites Thr^{906} (p-value for NEM or staurosporine: $p = 0.0026$) and Thr^{1007} (p-value for NEM or staurosporine: $p = 0.0026$) of *rn*KCC2 and Thr$^{203/207/212}$ of *hs*NKCC1 (p-value for NEM and staurosporine:

Table 4. Phospho-sites of *hs*PKC endogenously expressed in stably transfected HEK^{rnKCC2b} cells. Stably transfected HEK^{rnKCC2b} were treated with or without 1 mM NEM or 8 μM staurosporine before they were analyzed by mass spectrometry. The protein accession numbers are: *hs*PKC Alpha (P17252), *hs*PKC Beta (P05771-2), *hs*PKC Delta (Q05655), *hs*PKC Epsilon (Q02156), *hs*PKC Theta (Q04759), *hs*PKC Eta (P24723), and *hs*PKC Iota (P41743).

classes	sample	Phosphorylation site	Phosphopeptides	untreated	staurosporine treated	NEM treated
conventional	**PKC Alpha**	10;11	ADVFPGND**ST**ASQDVANRFARK	(3)		(1)
		10;13	ADVFPGND**ST**ASQDVANRFARK	(3) (3)	(1) (1)	(1) (1)
		226	TIRSTLNPQWNE**S**FTFK		(2)	(2)
		319	VI**S**PSEDRK	(3) (3)	(3) (2)	(2) (3)
	PKC Beta	11	ADPAAGPPP**S**EGEESTVRFARK	(2)	(1)	(2)
		641	HPPVL**T**PPDQEVIR	(3)	(3)	(3)
novel	**PKC Delta**	645	ARL**S**YSDK	(3)	(3)	(3)
		647	ARLSY**S**DK	(2)	(1)	(1)
		664	NLIDSMDQSAFAGF**S**FVNPK	(1)		(3)
	PKC Epsilon	309	VLADLGV**T**PDK	(2)	(2)	(2)
	PKC Theta	685	ALIN**S**MDQNMFR	(2)	(1)	(2)
	PKC Eta	317	TLAGMGLQPGNI**S**PTSK	(3)	(2)	(2)
atypical	**PKC Iota**	564	PNISGEFGLDNFDSQFTNEPVQL**T**PDDDDIVRK	(3)	(1)	(3)

The number in brackets indicates in how many technical replica a given phospho-site was detected (max. 3). Each bracket provides the results of one biological experiment.

https://doi.org/10.1371/journal.pone.0232967.t004

$p = 0.0026$) [72–75, 103]. The reduced phosphorylation of Thr^{212} in *hs*NKCC1 agrees with our phosphoproteome analyses as no phosphorylation of Thr^{212}/Thr^{217} in NKCC1 was observed (Table 1).

Previous analyses showed that SPAK directly phosphorylates Thr^{1007} of *rn*KCC2 [48] and Thr$^{203/207/212}$ of *hs*NKCC1 [70]. Treatment of HEK293 cells with NEM resulted in a decrease of phosphorylation of Thr^{233} ($p = 0{,}0026$), that is located in the T-loop kinase domain, and the S-loop phosphorylation site Ser^{373} of *hs*SPAK ($p = 0.0026$) (Fig 3). Both are targets of WNKs [48, 69, 93]. As no data were available for the staurosporine mediated effect, we additionally analyzed its impact on these phospho-sites in HEK293 cells. Staurosporine also reduced the phosphorylation of Thr^{233} ($p = 0.0026$) and Ser^{373} ($p = 0.0026$) in *hs*SPAK (Fig 3). Thus, both agents reduced phosphorylation levels of these SPAK phospho-sites. These data conform well to our phosphoproteomic analyses, as no phosphorylated Ser$^{372/373}$ of *hs*SPAK was detected after treatment with either of the two agents.

Furthermore, staurosporine reduced phosphorylation of Ser^{940} ($p = 0.0026$) in HEK^{rnKCC2b}, whereas NEM increased phosphorylation of Ser^{940} ($p = 0.046$) significantly (Fig 3). Since, Ser^{940} is directly phosphorylated by PKC [77, 104], we here analyzed the impact of both agents on the T-loop phosphorylation site Thr^{505} of PKC-δ. Autophosphorylation of this site is most probably essential for kinase activity [105–107]. Staurosporine significantly decreases Thr^{505} phosphorylation ($p = 0.0026$, Fig 3), whereas NEM slightly, but not significantly, increases Thr^{505} phosphorylation ($p = 0.064$). The different impact of both agents on the phosphorylation of Thr^{505} of PKC correlates well with their impact on Ser^{940} phosphorylation of KCC2b.

We also determined whether staurosporine or NEM altered the total protein amount of *rn*KCC2b, *hs*NKCC1 or *hs*SPAK (Fig 3). Whereas NEM resulted in increased KCC2 amount ($p = 0.0026$), no obvious change was detected upon staurosporine treatment. NKCC1 and SPAK levels were not changed significantly upon treatment with either agent.

To conclude, staurosporine and NEM reduced the phosphorylation status of SPAK (Thr^{233} and Ser^{373}). This correlated with the reduction of the phosphorylation of Thr^{1007} in *rn*KCC2b

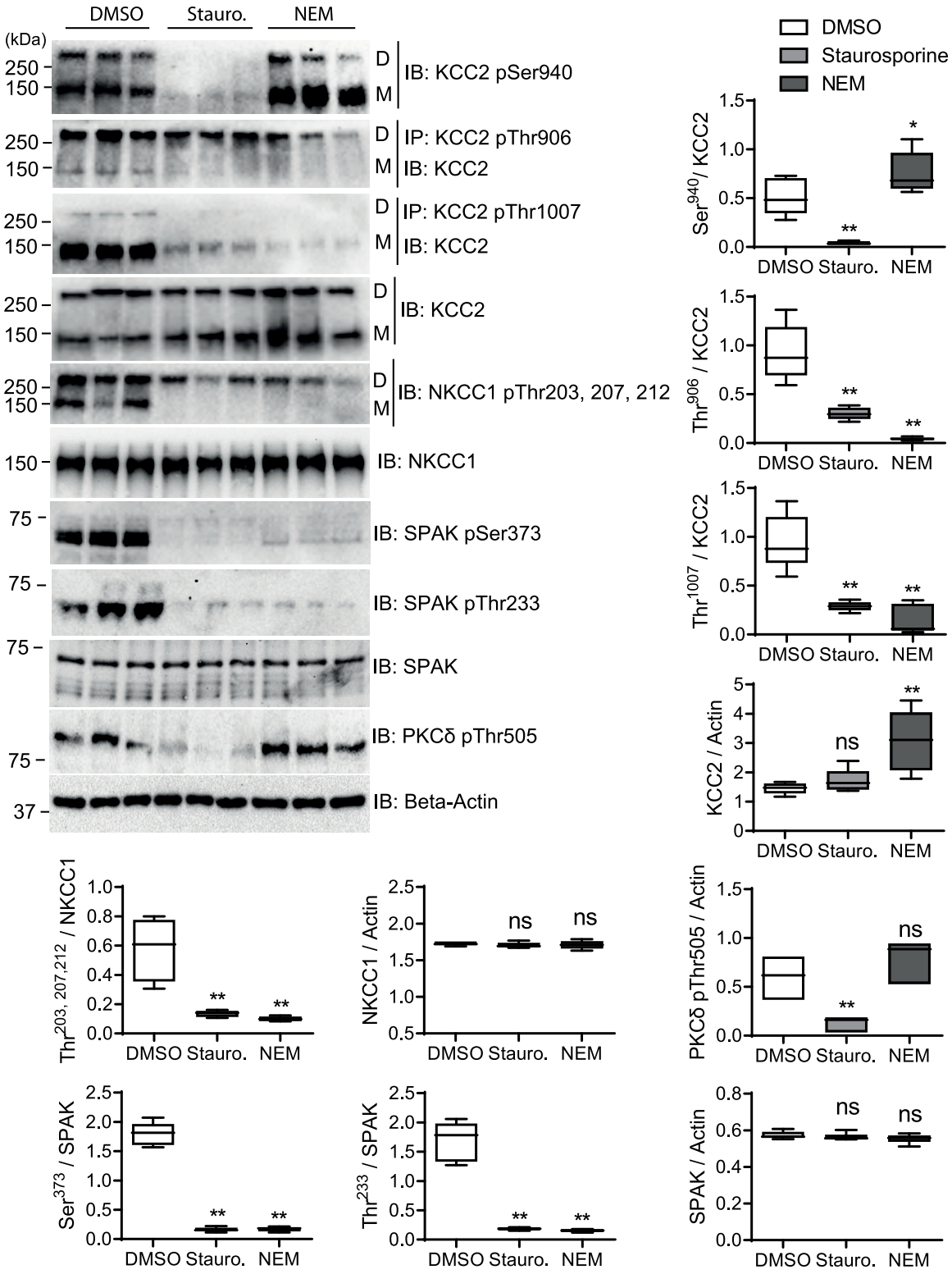

Fig 3. Quantitative analyses of *rn*KCC2b and *hs*NKCC1 phospho-sites upon staurosporine and NEM treatment in HEK^{rnKCC2b} cells. Stably transfected HEK^{rnKCC2b} cells were treated with DMSO (control), 8 μM staurosporine or 0.5 mM NEM, respectively, for 15 min. Cell lysates were harvested and subjected to immunoprecipitation (IP) and immunoblot (IB) with indicated antibodies. D, dimeric KCC2; M, monomeric KCC2. Band intensities were quantified with ImageJ software. ***, $p < 0.001$; **, $p < 0.01$; Wilcoxon-Mann-Whitney test (n = 6).

https://doi.org/10.1371/journal.pone.0232967.g003

and Thr$^{203/207/212}$ in *hs*NKCC1. Additionally, both agents reduced phosphorylation of Thr^{906} in *rn*KCC2b, which is phosphorylated by WNKs and a yet unknown kinase [48]. Staurosporine also reduced phosphorylation of the PKC site Ser^{940} in *rn*KCC2b, whereas NEM increased its phosphorylation level. This correlated with the reduction of Thr^{505} phosphorylation of PKC-δ upon staurosporine treatment and the impact of NEM to increase Thr^{505} phosphorylation.

Quantitative analyses of phospho-sites of KCC2 and NKCC1 upon staurosporine or NEM treatment of rat immature hippocampal neurons

As KCC2 is predominantly expressed in neurons [20], we analyzed for the first time the impact of staurosporine and NEM on the phosphorylation of specific phospho-sites of endogenously expressed KCC2 and NKCC1 using immature (9 DIV) primary rat hippocampal neurons (Fig 4). At this age cultured hippocampal neurons exhibit prominent level of Thr^{906} and Thr^{1007} KCC2 phosphorylation [66] that could be a subject of modulation by staurosporine and NEM. To this end, we treated neurons with 8 μM staurosporine, 0.5 mM NEM or DMSO as a vehicle control for 15 min. NEM was reduced to 0.5 mM, since higher concentrations induced cell death. As described for the analyses in stably transfected HEK^{rnKCC2b} cells, we used phospho-specific KCC2 and NKCC1 antibodies to quantify phosphorylation levels of each phospho-site relatively to the DMSO control. In untreated cultured immature hippocampal neurons, Ser^{940}, Thr^{906} and Thr^{1007} in KCC2 and Thr$^{203,\ 207,\ 212}$ in NKCC1 were phosphorylated, similar to stably transfected HEK^{rnKCC2b} cells (Fig 4).

Most actions of staurosporine and NEM, as monitored by immunblots, were similar between HEK^{rnKCC2b} cells and immature hippocampal neurons. Both agents resulted in decreased phosphorylation of Thr^{1007} in KCC2 (p-value for NEM and staurosporine: $p = 0.0026$), Thr$^{203/207/212}$ in NKCC1 (p-value for NEM and staurosporine: $p = 0.0026$), and Ser^{373} in SPAK (p-value for NEM: $p = 0.0026$ and staurosporine: $p = 0.0026$). Additionally, both agents reduced phosphorylation of the WNK-dependent phospho-site Thr^{906} in KCC2 (p-value for NEM and staurosporine: $p = 0.0026$). Finally, NEM increased the total protein level of KCC2, as observed in HEK293 cells ($p = 0.015$) (Fig 4). We were not able to detect the phosphorylation of Thr^{233} of SPAK using phospho-specific antibodies.

A marked difference, however, was observed for the PKC dependent phospho-site Ser^{940}. Here, treatment with NEM reduced phosphorylation of Ser^{940} ($p = 0.0026$) (Fig 4), contrary to the results obtained in stably transfected HEK^{rnKCC2b} cells (Fig 3). Treatment with staurosporine also resulted in reduced phosphorylation of Ser^{940} ($p = 0.0026$), which was similar to its action in HEK^{rnKCC2b} cells. We could not detect Thr^{505} phosphorylation of PKC-δ due to low expression rates.

To sum up, NEM affected the phosphorylation status of Ser^{940} in immature hippocampal neurons (decrease) in the opposite way compared to HEK^{rnKCC2b} cells (increase). All other effects of staurosporine and NEM were similar between immature hippocampal neurons and HEK293 cells, i.e. both reduced the phosphorylation status of Ser^{940}, Thr^{906}, and Thr^{1007} in KCC2 and Thr$^{203/207/212}$ in *hs*NKCC1.

Discussion

KCC2 and NKCC1 are key players for the development and maintenance of fast inhibitory neurotransmission. Their oppositely directed transport of K^+ and Cl^- ions within the same neuronal population necessitates a precisely coordinated regulatory mechanism for efficient setting of the intracellular [Cl^-] concentration [4, 38, 55–60] (Fig 5).

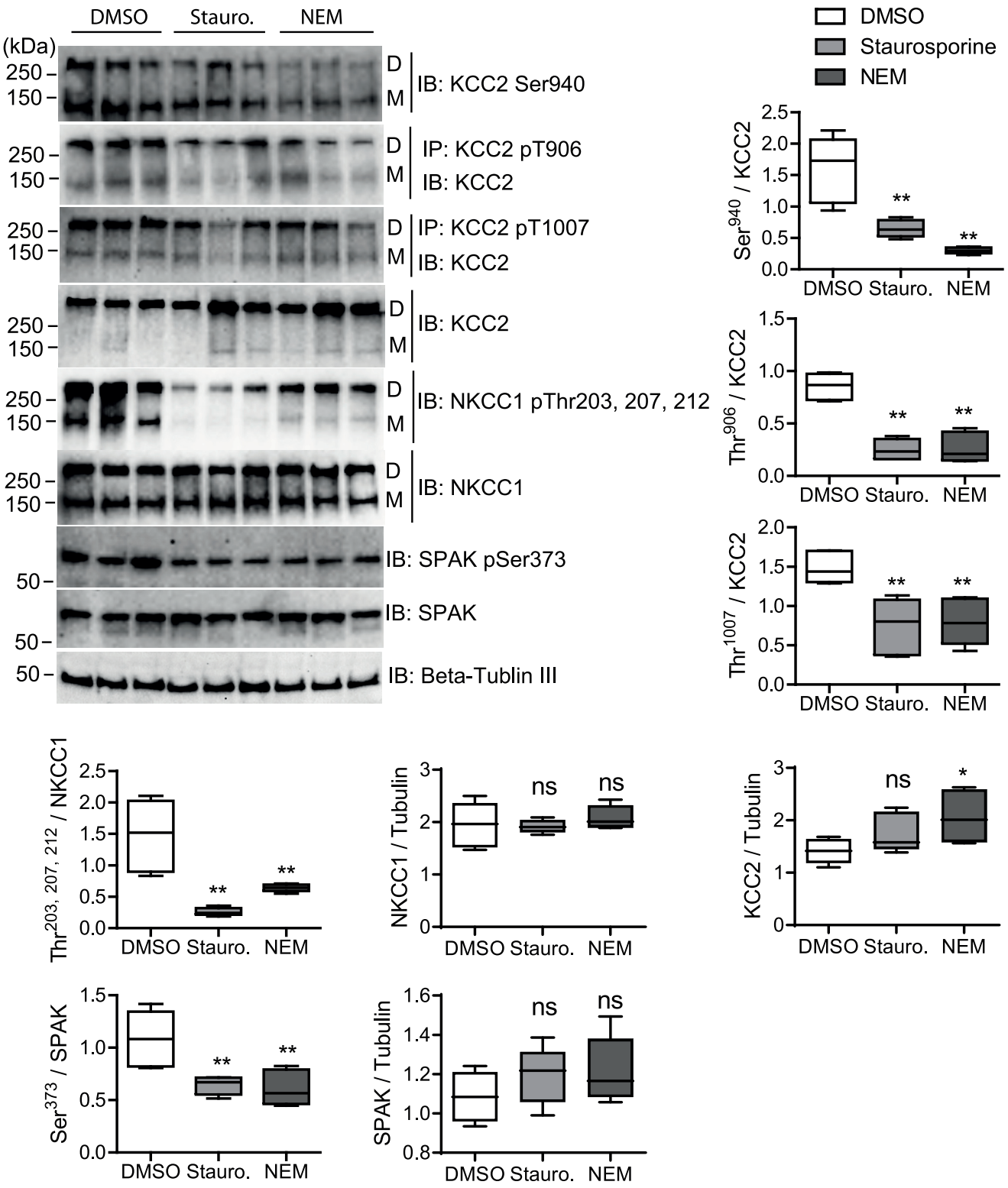

Fig 4. Quantitative analyses of *rn*KCC2 and *rn*NKCC1 phospho-sites upon staurosporine or NEM treatment in immature hippocampal neurons. Immature rat hippocampal neurons were treated with DMSO (control), 8 μM staurosporine or 0.5 mM NEM, respectively, for 15 min. Neuronal lysates were harvested and subjected to immunoprecipitation (IP) and immunoblot (IB) with the indicated antibodies. D, dimeric KCC2; M, monomeric KCC2. Band intensities were quantified using ImageJ software. ***, $p < 0.001$; **, $p < 0.01$; Wilcoxon-Mann-Whitney test (n = 6).

https://doi.org/10.1371/journal.pone.0232967.g004

Posttranslational regulation via the WNK-SPAK/OSR1 dependent phosphorylation represents a potent mechanism to regulate transport activity of KCC2 and NKCC1 in a reciprocal way [60, 108–110] (Fig 5). Here, we show that staurosporine and NEM decrease phosphorylation of Thr^{233} and Ser^{373} in SPAK, of Thr^{1007} in *rn*KCC2 and Thr^{203}, Thr^{207} and Thr^{212} in *hs*NKCC1 in both HEK293 cells and immature cultured hippocampal neurons. Since SPAK directly impairs phosphorylation of Thr^{1007} in *rn*KCC2 and Thr^{203}, Thr^{207} and Thr^{212} in *hs*NKCC1 [38, 48, 59, 60, 63, 68–76], our data suggest that staurosporine and NEM directly affect the WNK-SPAK/OSR1 mediated phosphorylation of these residues in KCC2 and NKCC1. The data are in line with previous analyses showing that NEM reduces phosphorylation of Ser^{373} in SPAK and Thr^{1007} in KCC2 using HEK293 cells and immature cortical neurons [48]. Furthermore, application of staurosporine and NEM decreases phosphorylation of Thr^{906} in *rn*KCC2. This site is directly phosphorylated by WNKs and a yet unknown kinase [48]. However, functional in-depth analyses such as mutagenic approaches are required to prove a causal relation between dephosphorylation of SPAK Thr^{233} and Ser^{373} and dephosphorylation of the specific KCC2 and NKCC1 phospho-sites upon staurosporine and NEM treatment.

Recent analyses demonstrated that dephosphorylation of Thr^{906} and Thr^{1007} increases KCC2 activity [61, 64–66], whereas dephosphorylation of Thr^{203}, Thr^{207} and Thr^{212} decreases NKCC1 activity [45, 51]. Furthermore, staurosporine and NEM results in activation of KCC2 (this study and [40, 47, 48, 59, 60, 79, 80], whereas they reduce NKCC1 activity [43–46, 51]. This suggests, that staurosporine and NEM mediated dephosphorylation of these phosphosites result in a reciprocal regulation of KCC2 (activation) and NKCC1 (inactivation) activity most likely via the WNK/SPAK-dependent phosphorylation pathway. This is also in line with the observation in immature hippocampal neurons that KCC2 can rapidly be activated by staurosporine [42].

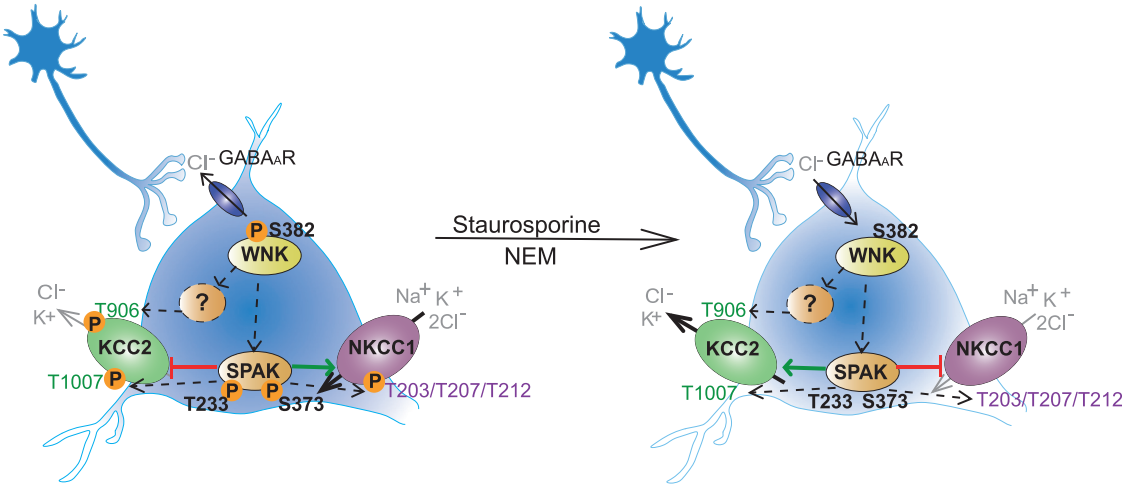

Fig 5. Staurosporine and NEM impair the WNK-SPAK/OSR1 mediated phosphorylation of KCC2 and NKCC1. In immature hippocampal neurons, the WNK mediated phosphorylation of SPAK/OSR1 directly phosphorylates T^{1007} of KCC2 and T^{203}, T^{207} and T^{212} of NKCC1. WNKs also interact with a yet unknown kinase to phosphorylate Thr^{906} of KCC2. Phosphorylation of these residues decreases KCC2 and increases NKCC1 activity. Application of staurosporine or NEM decreases phosphorylation of S^{382} of WNK1 and T^{233} and S^{373} of SPAK. This likely results in reduction of phosphorylation of T^{906} and T^{1007} in KCC2 and of T^{203}, T^{207} and T^{212} in NKCC1. Dephosphorylation of these residues increases KCC2 activity and decreases NKCC1 activity. The figure is modified from Moore et al. [39].

https://doi.org/10.1371/journal.pone.0232967.g005

Another key regulatory KCC2 phospho-site is the PKC-mediated phosphorylation of Ser^{940}. Phosphorylation of Ser^{940} enhances KCC2 cell surface expression and increases ion transport activity, whereas mutation of serine to alanine (mimicking the dephosphorylated state) results in transport activity that is equal or decreased compared to wild-type KCC2 ($KCC2^{wt}$) [65, 77, 111]. Our data demonstrate that staurosporine and NEM can differentially affect Ser^{940} phosphorylation. Treatment of immature hippocampal neurons with either agent results in decreased phosphorylation of Ser^{940}. However, treatment of $HEK^{rnKCC2b}$ cells with staurosporine decreases, whereas NEM increases phosphorylation of Ser^{940}. This is in line with the different effect of these agents on transport activity of the phosphomutants $Ser^{31A/D}$, $Thr^{34A/D}$, Thr^{999A} and $Thr^{1008A/D}$ [40].

Moreover, NEM has a cell-type specific impact on Ser^{940} phosphorylation. In immature cortical neurons [48] and HEK293 cells, NEM increases Ser^{940} phosphorylation, whereas it decreases Ser^{940} phosphorylation in immature cultured hippocampal neurons (Fig 4). The mechanisms that cause this opposite effect of NEM on Ser^{940} phosphorylation in different tissues is unclear. One possibility is that different NEM concentrations (HEK293 cells: 1 mM and 0.1 mM; immature hippocampal neurons: 0.5 mM; immature cortical neurons: 0.1 mM [48]) affect different regulatory pathways. Alternatively, tissues-specific sets of PKC isoforms and phosphatases result in different phosphorylation patterns. Indeed, the PKC family consists of 10–12 isoforms grouped into three classes [98–101] that vary in their expression profile [112] and regulation of their activity through several regulatory proteins, co-factors and second messenger cascades [100, 101, 113]. This offers the opportunity to differentially regulate KCC2 function in distinct neuronal populations through PKC. In $HEK^{rnKCC2b}$ cells, we showed that staurosporine reduced and NEM slightly increased phosphorylation of the T-loop phospho-site Thr^{505} of PKC-δ. This correlated with decreased KCC2 Ser^{940} phosphorylation upon staurosporine treatment and increased phosphorylation of this residue upon NEM treatment. This suggests, that both agents directly act on PKC-δ mediating the phosphorylation of Ser^{940} in $HEK^{rnKCC2b}$ cells. However, more functional in-depth analyses are required to elucidate the causal link between dephosphorylation of PKC-δ Thr^{505} and dephosphorylation of KCC2 Ser^{940} upon staurosporine treatment. Since we were unable to detect phosphorylation of PKC-δ Thr^{505} in immature hippocampal neurons, we suggest that other PKC isoforms are involved in the direct phosphorylation of KCC2 Ser^{940} in immature hippocampal neurons.

Our data furthermore reveal that staurosporine ($HEK^{rnKCC2b}$ cells, immature hippocampal neurons) and NEM treatment (immature hippocampal neurons) decrease Ser^{940} phosphorylation resulting in an equal or diminished transport activity compared to $KCC2^{wt}$ [65, 77, 111]. We therefore conclude that Ser^{940} is not the key regulatory phospho-site mediating the staurosporine and NEM-based stimulation effect on KCC2. This is in line with recent published analyses showing that NEM still enhances the transport activity of Ser^{940A} (mimicking dephosphorylated state), indicating that other phospho-sites are important in NEM-dependent stimulation [40, 48].

NEM but not staurosporine increased total KCC2 amount in HEK293 cells and immature cultured hippocampal neurons. In immature cortical neurons, Deep and coworkers [48] detected the same trend of enhanced total KCC2 abundance (albeit not significant), resulting in increased cell surface expression [48]. This suggests that in contrast to staurosporine, NEM increases KCC2 expression and trafficking that could result in a higher KCC2 activity. The different impact of NEM on total KCC2 abundance in HEK293 in the study of Deep and coworkers (no increase) and our analyses (increase) could result from different NEM concentration used in the experiments (0.1 mM vs. 1 mM).

Via mass spectrometry analysis, we identified several new phosphorylation sites whose function awaits further investigation. These sites are the N-terminal KCC2 phospho-site Thr^{32}, and the C-terminal NKCC1 phospho-sites Ser^{242}, Thr^{266}, Th^{268}, Ser^{940}, Tyr^{956} and

Ser^{957}. Future studies should investigate their regulatory impact on KCC2 and NKCC1 activity.

Conclusions

In conclusion, our data identify molecular mechanisms involved in staurosporine and NEM mediated changes in transport activity of KCC2 and NKCC1, which are a defining feature of CCCs [114]. The observation of cell-type specific action of these agents is in line with different reversal potentials in mature neuronal populations [115] and calls for comprehensive neuron sub-type-specific phospho analysis. The recently reported structural data of CCCs [116–119] finally lay the foundation to analyze jointly the physiological role of phosphorylation and underlying structural changes to obtain an integrative and mechanistic view of the action of phosphorylation.

Supporting information

S1 Table. Phospho-sites in PhosphoSitePlus detected by mass spectrometry analyses.
(DOCX)

S2 Table. Phospho-sites in PhosphoSitePlus detected by mass spectrometry analyses.
(DOCX)

S3 Table. Phospho-sites in PhosphoSitePlus detected by mass spectrometry analyses.
(DOCX)

S1 Fig. Quantitative analyses of *rn*KCC2 and *hs*NKCC1 phospho-sites upon staurosporine and NEM treatment in HEK^{rnKCC2b} cells.
(PDF)

S2 Fig. Quantitative analyses of *rn*KCC2 and *hs*NKCC1 phospho-sites upon staurosporine and NEM treatment in immature hippocampal neurons.
(PDF)

Acknowledgments

We thank M. Reents for excellent technical support. Authors are also grateful to Prof. Matthias Mann for continuous support and Katharina Zettl for technical support.

Author Contributions

Conceptualization: Igor Medina, Anna-Maria Hartmann.

Data curation: Jinwei Zhang, Antje Cordshagen, Igor Medina, Jacek R. Wisniewski, Michael Winklhofer, Anna-Maria Hartmann.

Formal analysis: Jinwei Zhang, Antje Cordshagen, Jacek R. Wisniewski, Michael Winklhofer, Anna-Maria Hartmann.

Funding acquisition: Hans Gerd Nothwang, Jacek R. Wisniewski, Anna-Maria Hartmann.

Investigation: Jinwei Zhang, Antje Cordshagen, Igor Medina, Jacek R. Wisniewski, Anna-Maria Hartmann.

Methodology: Jinwei Zhang, Antje Cordshagen, Igor Medina, Jacek R. Wisniewski, Michael Winklhofer, Anna-Maria Hartmann.

Project administration: Hans Gerd Nothwang, Anna-Maria Hartmann.

Supervision: Igor Medina, Hans Gerd Nothwang, Jacek R. Wisniewski, Anna-Maria Hartmann.

Validation: Jinwei Zhang, Antje Cordshagen, Igor Medina, Jacek R. Wisniewski, Michael Winklhofer, Anna-Maria Hartmann.

Visualization: Jinwei Zhang, Antje Cordshagen, Jacek R. Wisniewski, Michael Winklhofer, Anna-Maria Hartmann.

Writing – original draft: Jinwei Zhang, Igor Medina, Hans Gerd Nothwang, Jacek R. Wisniewski, Michael Winklhofer, Anna-Maria Hartmann.

References

1. Hartmann A-M, Tesch D, Nothwang HG, Bininda-Emonds ORP. Evolution of the Cation Chloride Cotransporter Family: Ancient Origins, Gene Losses, and Subfunctionalization through Duplication. Molecular biology and evolution. 2014:mst225.
2. Gamba G. Molecular Physiology and Pathophysiology of electroneutral Cation-Chloride Cotransporter. Physiological Reviews. 2005; 85:423–93. https://doi.org/10.1152/physrev.00011.2004 PMID: 15788703
3. Daigle ND, Carpentier GA, Frenette-Cotton R, Simard CF, Lefoll M-H, Noel M, et al. Molecular characterization of a human cation-Cl- cotransporter (SLC12A8, CCC9A) that promotes polyamine and amino acid transport. Journal of Cellular Physiology. 2009; 220:680–9. https://doi.org/10.1002/jcp.21814 PMID: 19472210
4. Hartmann A, Nothwang HG. Molecular and evolutionary insights into the structural organization of cation chloride cotransporters. Name: Frontiers in Cellular Neuroscience. 2015; 8:470. https://doi.org/10.3389/fncel.2014.00470 PMID: 25653592
5. Payne JA, Rivera C, Voipo J, Kaila K. Cation-Chloride cotransporters in neuronal communication, development and trauma Trends in Neuroscience. 2003; 26:199–206.
6. Arroyo JP, Kahle KT, Gamba G. The SLC12 family of electroneutral cation-coupled chloride cotransporters. Molecular Aspects of Medicine. 2013; 34:288–98. https://doi.org/10.1016/j.mam.2012.05.002 PMID: 23506871
7. Kahle KT, Staley KJ, Nahed BV, Gamba G, Hebert SC, Lifton RP, et al. Roles of the cation-chloride cotransporters in neurological disease. Nature Clinical Practice. 2008; 4:490–502.
8. Blaesse P, Airaksinen MS, Rivera C, Kaila K. Cation-Chloride Cotransporters and Neuronal Function. Cell. 2009; 61:820–38.
9. Adragna NC, Fulvio MD, Lauf PK. Regulation of K-Cl Cotransport: from Function to Genes. Journal of Membrane Biology. 2004; 201:109–37. https://doi.org/10.1007/s00232-004-0695-6 PMID: 15711773
10. Di Fulvio M, Alvarez-Leefmans FJ. The NKCC and NCC genes: an in silico view. Physiology and Pathology of Chloride Transporters and Channels in the Nervous System. 2009:169–208.
11. Gagnon KB, Delpire E. Physiology of SLC12 transporters: lessons from inherited human genetic mutations and genetically engineered mouse knockouts. American Journal of Physiology-Cell Physiology. 2013; 304:C693–C714. https://doi.org/10.1152/ajpcell.00350.2012 PMID: 23325410
12. Medina I, Friedel P, Rivera C, Kahle KT, Kourdougli N, Uvarov P, et al. Current view on the functional regulation of the neuronal K+-Cl− cotransporter KCC2. Frontiers in cellular neuroscience. 2014;8.
13. Achilles K, Okabe A, Ikeda M, Shimizu-Okabe C, Yamada F, Fukuda A, et al. Kinetic properties of Cl^- uptake mediated by Na^+-dependent K^+-$2Cl^-$ cotransport in immature rat neocortical neurons. Journal of Neuroscience. 2007; 27:8616–27. https://doi.org/10.1523/JNEUROSCI.5041-06.2007 PMID: 17687039
14. Sipilä ST, Huttu K, Yamada J, Afzalov R, Voipio J, Blaesse P, et al. Compensatory enhancement of intrinsic spiking upon NKCC1 disruption in neonatal hippocampus. The Journal of Neuroscience. 2009; 29:6982–8. https://doi.org/10.1523/JNEUROSCI.0443-09.2009 PMID: 19474325
15. Yamada J, Okabe M, Toyoda H, Kilb W, Luhmann HJ, Fukuda A. Cl^- uptake promoting depolarizing GABA actions in immature rat neocortical neurones is mediated by NKCC1. Journal of Physiology. 2004; 557:829–41. https://doi.org/10.1113/jphysiol.2004.062471 PMID: 15090604
16. Yuste R, Katz LC. Control of postsynaptic Ca^{2+} influx in developing neocortex by excitatory and inhibitory neurotransmitters. Neuron. 1991; 6:333–44. https://doi.org/10.1016/0896-6273(91)90243-s PMID: 1672071

17. Reichling DB, Kyrozis A, Wang J, MacDermott AB. Mechanism of GABA and glycine depolarization-induced calcium transients in rat dorsal horn neurons. Journal of Physiology. 1994; 476:411–21. https://doi.org/10.1113/jphysiol.1994.sp020142 PMID: 8057250

18. Owens DF, Boyce LH, Davis MBE, Kriegstein AR. Excitatory GABA responses in embryonic and neonatal cortical slices demonstrated by gramicidin perforated-patch recordings and calcium imaging. The Journal of Neuroscience. 1996; 16:6416–23.

19. Hübner CA, Stein V, Hermans-Borgmeyer I, Meyer T, Ballanyi K, Jentsch TJ. Disruption of KCC2 reveals an essential role of K-Cl cotransport already in early synaptic inhibition. Neuron. 2001; 30:515–24. https://doi.org/10.1016/s0896-6273(01)00297-5 PMID: 11395011

20. Uvarov P, Ludwig A, Markkanen M, Pruunsild P, Kaila K, Delpire E, et al. A novel N-termianl isoform of the neuron-specific K-Cl Cotransporter KCC2. Journal of Biological Chemistry. 2007; 282(42):30570–6. https://doi.org/10.1074/jbc.M705095200 PMID: 17715129

21. Kim JY, Liu CY, Zhang F, Duan X, Wen Z, Song J, et al. Interplay between DISC1 and GABA signaling regulates neurogenesis in mice and risk for schizophrenia. Cell. 2012; 148(5):1051–64. https://doi.org/10.1016/j.cell.2011.12.037 PMID: 22385968

22. Tyzio R, Nardou R, Ferrari DC, Tsintsadze T, Shahrokhi A, Eftekhari S, et al. Oxytocin-mediated GABA inhibition during delivery attenuates autism pathogenesis in rodent offspring. Science. 2014; 343(6171):675–9. https://doi.org/10.1126/science.1247190 PMID: 24503856

23. Kahle KT, Merner ND, Friedel P, Silayeva L, Liang B, Khanna A, et al. Genetically encoded impairment of neuronal KCC2 cotransporter function in human idiopathic generalized epilepsy. EMBO reports. 2014; 15(7):766–74. https://doi.org/10.15252/embr.201438840 PMID: 24928908

24. Merner ND, Chandler MR, Bourassa C, Liang B, Khanna AR, Dion P, et al. Regulatory domain or CpG site variation in SLC12A5, encoding the chloride transporter KCC2, in human autism and schizophrenia. Frontiers in cellular neuroscience. 2015;9. https://doi.org/10.3389/fncel.2015.00009 PMID: 25698924

25. Huberfeld G, Wittner L, Clemenceau S, Baulac M, Kaila K, Miles R, et al. Perturbed chloride homeostasis and GABAergic signaling in human temporal lobe epilepsy. The Journal of Neuroscience. 2007; 27(37):9866–73. https://doi.org/10.1523/JNEUROSCI.2761-07.2007 PMID: 17855601

26. Coull JAM, Boudreau D, Bachand K, Prescott SA, Nault F, Sik A, et al. Trans-synaptic shift in anion gradient in spinal lamina I neurons as a mechanism of neuropathic pain. Nature. 2003; 424:938–42. https://doi.org/10.1038/nature01868 PMID: 12931188

27. Rivera C, Li H, Thomas-Crussels J, Lahtinen H, Viitanen T, Nanobashvili A, et al. BDNF-induced TrkB activation down-regulates the K+-Cl- cotransporter KCC2 and impairs neuronal Cl- extrusion. The Journal of Cell Biology. 2002; 159(5):747–52. https://doi.org/10.1083/jcb.200209011 PMID: 12473684

28. Boulenguez P, Liabeuf S, Bos R, Bras H, Jean-Xavier C, Brocard C, et al. Down-regulation of the potassium-chloride cotransporter KCC2 contributes to spasticity after spinal cord injury. Nature medicine. 2010; 16(3):302–7. https://doi.org/10.1038/nm.2107 PMID: 20190766

29. Papp E, Rivera C, Kaila K, Freund TF. Relationship between neuronal vulnerability and potassium-chloride cotransporter 2 immunreactivity in hippocampus following transient forebrain ischemia. 2008. 2008;Neuroscience:677–89.

30. Shulga A, Thomas-Crusells J, Sigl T, Blaesse A, Mestres P, Meyer M, et al. Posttraumatic GABAA-mediated [Ca2+] i increase is essential for the induction of brain-derived neurotrophic factor-dependent survival of mature central neurons. The Journal of Neuroscience. 2008; 28(27):6996–7005. https://doi.org/10.1523/JNEUROSCI.5268-07.2008 PMID: 18596173

31. Puskarjov M, Ahmad F, Khirug S, Sivakumaran S, Kaila K, Blaesse P. BDNF is required for seizure-induced but not developmental up-regulation of KCC2 in the neonatal hippocampus. Neuropharmacology. 2014.

32. Pisella LI, Gaiarsa J-L, Diabira D, Zhang J, Khalilov I, Duan J, et al. Impaired regulation of KCC2 phosphorylation leads to neuronal network dysfunction and neurodevelopmental pathology. 2019; 12(603): eaay0300.

33. Delpire E, Lu J, England R, Dull C, Thorne T. Deafness and imbalance associated with inactivation of the secretory Na-K-2Cl co-transporter. Nature Genetics. 1999; 22:192–5. https://doi.org/10.1038/9713 PMID: 10369265

34. Delpire E, Mount DB. Human and Murine Phenotypes associated with defects in Cation-Chloride-Cotransporter. Annu Rev Physiol. 2002; 64:803–43. https://doi.org/10.1146/annurev.physiol.64.081501.155847 PMID: 11826289

35. Dzhala VI, Talos DM, Sdrulla DA, Brumback AC, Mathews GC, Benke TA, et al. NKCC1 transporter facilates seizures in the developing brain. Nature Medicine. 2005; 11:1205–13. https://doi.org/10.1038/nm1301 PMID: 16227993

36. Zhu L, Polley N, Mathews GC, Delpire E. NKCC1 and KCC2 prevent hyperexcitability in the mouse hippocampus. Epilepsy research. 2008; 79(2–3):201–12. https://doi.org/10.1016/j.eplepsyres.2008.02.005 PMID: 18394864

37. Ben-Ari Y. NKCC1 chloride importer antagonists attenuate many neurological and psychiatric disorders. Trends in neurosciences. 2017; 40(9):536–54. https://doi.org/10.1016/j.tins.2017.07.001 PMID: 28818303

38. Alessi DR, Zhang J, Khanna A, Hochdörfer T, Shang Y, Kahle KT. The WNK-SPAK/OSR1 pathway: Master regulator of cation-chloride cotransporters. Science signaling. 2014; 7(334):re3–re. https://doi.org/10.1126/scisignal.2005365 PMID: 25028718

39. Moore YE, Kelley MR, Brandon NJ, Deeb TZ, Moss SJJTin. Seizing control of KCC2: a new therapeutic target for epilepsy. 2017; 40(9):555–71.

40. Cordshagen A, Busch W, Winklhofer M, Nothwang HG, Hartmann A-M. Phosphoregulation of the intracellular termini of K+-Cl− cotransporter 2 (KCC2) enables flexible control of its activity. Journal of Biological Chemistry. 2018; 293(44):16984–93. https://doi.org/10.1074/jbc.RA118.004349 PMID: 30201606

41. Blaesse P, Guillemin I, Schindler J, Schweizer M, Delpire E, Khiroug L, et al. Oligomerization of KCC2 Correlates with Development of Inhibitory Neurotransmission. The Journal of Neuroscience. 2006; 26 (41):10407–19. https://doi.org/10.1523/JNEUROSCI.3257-06.2006 PMID: 17035525

42. Khirug S, Huttu K, Ludwig A, Smirnov S, Voipo J, Rivera C, et al. Distinct properties of functional KCC2 expression in immature mouse hippocampal neurons in culture and in acute slices. European Journal of Neuroscience. 2005; 21(4):899–904. https://doi.org/10.1111/j.1460-9568.2005.03886.x PMID: 15787696

43. Flatman PW. Regulation of Na-K-2Cl cotranport by phosphorylation adn protein-protein interactions. Biochemica et biophysica Acta. 2002; 1566:140–51.

44. Lytle C, McManus TJ, Haas M. A model of Na-K-2Cl cotransport based on ordered ion binding and glide symmetry. American Journal of Physiology-Cell Physiology. 1998; 274(2):C299–C309.

45. Muzyamba M, Cossins A, Gibson J. Regulation of Na+-K+-2Cl− cotransport in turkey red cells: the role of oxygen tension and protein phosphorylation. The Journal of physiology. 1999; 517(2):421–9.

46. Palfrey HC, Leung S. Inhibition of Na-K-2Cl cotransport and bumetanide binding by ethacrynic acid, its analogues, and adducts. American Journal of Physiology-Cell Physiology. 1993; 264(5):C1270–C7.

47. Weber M, Hartmann A-M, Beyer T, Ripperger A, Nothwang HG. A novel regulatory locus of phosphorylation in the C-terminus of the potassium chloride cotransporter KCC2 that interferes with N-ethylmaleimide or staurosporine mediated activation. Journal of Biological Chemistry. 2014:jbc-M114.

48. Conway LC, Cardarelli RA, Moore YE, Jones K, McWilliams LJ, Baker DJ, et al. N-Ethylmaleimide increases KCC2 cotransporter activity by modulating transporter phosphorylation. Journal of Biological Chemistry. 2017; 292(52):21253–63. https://doi.org/10.1074/jbc.M117.817841 PMID: 29092909

49. Bize I, Güvenç B, Buchbinder G, Brugnara C. Stimulation of human erythrocyte K-Cl cotransport and protein phosphatase type 2A by n-ethylmaleimide: role of intracellular Mg++. The Journal of membrane biology. 2000; 177(2):159–68. https://doi.org/10.1007/s002320001109 PMID: 11003690

50. Jennings ML, Schulz RK. Okadaic acid inhibition of KCl cotransport. Evidence that protein dephosphorylation is necessary for activation of transport by either cell swelling or N-ethylmaleimide. The Journal of general physiology. 1991; 97(4):799–817. https://doi.org/10.1085/jgp.97.4.799 PMID: 1647439

51. Gagnon KBE, England R, Delpire E. Characterization of SPAK and OSR1, regulatory kinases of the Na-K-2Cl cotransporter. Molecular and cellular biology. 2006; 26(2):689–98. https://doi.org/10.1128/MCB.26.2.689-698.2006 PMID: 16382158

52. Vardi N, Zhang L-L, Payne JA, Sterling P. Evidence that differnet cation chloride cotransporters in retinal neurons allow opposite responses to GABA. The Journal of Neuroscience. 2000; 20(20):7657–63. https://doi.org/10.1523/JNEUROSCI.20-20-07657.2000 PMID: 11027226

53. Balakrishnan V, Becker M, Löhrke S, Nothwang HG, Güresir E, Friauf E. Expression and Function of Chloride Transportes during Development of Inhibitory Neurotransmission in the Auditory Brainstem. The Journal of Neuroscience. 2003; 23:4134–45. https://doi.org/10.1523/JNEUROSCI.23-10-04134.2003 PMID: 12764101

54. Price TJ, Trussel LO. Estimate of the chloride concentration in a central glutamatergic terminal: gramicidin perforated-patch study on the calyx of Held. Journal of Neuroscience. 2006; 26:11432–6. https://doi.org/10.1523/JNEUROSCI.1660-06.2006 PMID: 17079672

55. Hartmann A-M, Blaesse P, Kranz T, Wenz M, Schindler J, Kaila K, et al. Opposite effect of membrane raft perturbation on transport activity of KCC2 and NKCC1. Journal of Neurochemistry. 2009; 111 (2):321–31. https://doi.org/10.1111/j.1471-4159.2009.06343.x PMID: 19686239

56. Wenz M, Hartmann A-M, Friauf E, Nothwang HG. CIP1 is an activator of the K^+-Cl^- cotransporter KCC2. Biochemical and Biophysical Research Communications. 2009; 381:388–92. https://doi.org/10.1016/j.bbrc.2009.02.057 PMID: 19232517

57. Caron L, Rousseau F, Gagnon É, Isenring P. Cloning and functional characterization of a cation-chloride cotransporter-interacting protein. J Biol Chem. 2000; 275:32027–36. https://doi.org/10.1074/jbc.M000108200 PMID: 10871601

58. De los Heros P, Kahle KT, Rinehart J, Bobadilla NA, Vázquez N, San-Cristobal P, et al. WNK3 bypasses the tonicity requirement for K-Cl cotransporter activation via a phosphatase-dependent pathway. PNAS. 2005; 103(6):1976–81.

59. Heubl M, Zhang J, Pressey JC, Al Awabdh S, Renner M, Gomez-Castro F, et al. GABA A receptor dependent synaptic inhibition rapidly tunes KCC2 activity via the Cl−-sensitive WNK1 kinase. Nature communications. 2017; 8(1):1776. https://doi.org/10.1038/s41467-017-01749-0 PMID: 29176664

60. Shekarabi M, Zhang J, Khanna AR, Ellison DH, Delpire E, Kahle KT. WNK kinase signaling in ion homeostasis and human disease. Cell metabolism. 2017; 25(2):285–99. https://doi.org/10.1016/j.cmet.2017.01.007 PMID: 28178566

61. Rinehart J, Maksimova YD, Tanis JE, Stone KL, Hodson CA, Zhang J, et al. Sites of Regulated Phosphorylation that Control K-Cl Cotransporter Activity. Cell. 2009; 138:525–36. https://doi.org/10.1016/j.cell.2009.05.031 PMID: 19665974

62. Markkanen M, Ludwig A, Khirug S, Pryazhnikov E, Soni S, Khiroug L, et al. Implications of the N-terminal heterogeneity for the neuronal K-Cl cotransporter KCC2 function. Brain research. 2017; 1675:87–101. https://doi.org/10.1016/j.brainres.2017.08.034 PMID: 28888841

63. De los Heros P, Alessi DR, Gourlay R, Campbell DG, Deak M, Macartney TJ, et al. The WNK-regulated SPAK/OSR1 kinases directly phosphorylate and inhibit the K^+-Cl^- co-transporters. Biochem J. 2014; 458:559–73. https://doi.org/10.1042/BJ20131478 PMID: 24393035

64. Moore YE, Deeb TZ, Chadchankar H, Brandon NJ, Moss SJ. Potentiating KCC2 activity is sufficient to limit the onset and severity of seizures. Proceedings of the National Academy of Sciences. 2018; 115 (40):10166–71.

65. Titz S, Sammler EM, Hormuzdi SG. Could tuning of the inhibitory tone involve graded changes in neuronal chloride transport? Neuropharmacology. 2015.

66. Friedel P, Kahle KT, Zhang J, Hertz N, Pisella LI, Buhler E, et al. WNK1-regulated inhibitory phosphorylation of the KCC2 cotransporter maintains the depolarizing action of GABA in immature neurons. Sci Signal. 2015; 8(383):ra65–ra. https://doi.org/10.1126/scisignal.aaa0354 PMID: 26126716

67. Inoue K, Furukawa T, Kumada T, Yamada J, Wang T, Inoue R, et al. Taurine inhibits K+-Cl− cotransporter KCC2 to regulate embryonic Cl− homeostasis via With-no-lysine (WNK) protein kinase signaling pathway. Journal of Biological Chemistry. 2012; 287(25):20839–50. https://doi.org/10.1074/jbc.M111.319418 PMID: 22544747

68. Hartmann A-M, Nothwang HG. Molecular and evolutionary insights into the structural organization of cation chloride cotransporters. Frontiers in cellular neuroscience. 2014; 8.

69. Richardson C, Alessi DR. The regulation of salt transport and blood pressure by the WNK-SPAK/OSR1 signalling pathway. Journal of cell science. 2008; 121(20):3293–304.

70. Thastrup JO, Rafiqi FH, Vitari AC, Pozo-Guisado E, Deak M, Mehellou Y, et al. SPAK/OSR1 regulate NKCC1 and WNK activity: analysis of WNK isoform interactions and activation by T-loop trans-autophosphorylation. Biochemical Journal. 2012; 441(1):325–37. https://doi.org/10.1042/BJ20111879 PMID: 22032326

71. Geng Y, Hoke A, Delpire E. The Ste20 Kinases SPAK and OSR1 regulate NKCC1 function in sensory neurons. The Journal of Biological Chemistry. 2009; 284:14020–8.

72. Gagnon KB, England R, Delpire E. A single binding motif is required for SPAK activation of the Na-K-2Cl cotransporter. Cellular Physiology and Biochemistry. 2007; 20(1–4):131–42. https://doi.org/10.1159/000104161 PMID: 17595523

73. Moriguchi T, Urushiyama S, Hisamoto N, Iemura S-I, Uchida S, Natsume T, et al. WNK1 regulates phosphorylation of Cation-Chloride-coupled Cotransporters via the STE20-related kinases, SPAK and OSR1. Journal of Biological Chemistry. 2005; 280(52):42685–93. https://doi.org/10.1074/jbc.M510042200 PMID: 16263722

74. Vitari AC, Thastrup J, Rafiqi FH, Deak M, Morrice Na, Karlsson H, K., et al. Functional interactions of the SPAK/OSR1 kinases with their upstream activator WNK1 and downstream substrate NKCC1. Biochemical Journal 2006; 397:223–31. https://doi.org/10.1042/BJ20060220 PMID: 16669787

75. Darman RB, Forbush B. A regulatory locus of phosphorylation in the N terminus of the Na-K-Cl cotransporter, NKCC1. Journal of Biological Chemistry. 2002; 277(40):37542–50. https://doi.org/10.1074/jbc.M206293200 PMID: 12145304

76. Dowd BFX, Forbush B. PASK (Proline-Alanine-rich-related Kinase), a regulatory kinase of the Na-K-Cl cotransporter (NKCC1). The Journal of Biological Chemistry. 2003; 278(30):27347–53. https://doi.org/10.1074/jbc.M301899200 PMID: 12740379

77. Lee HHC, Walker JA, Jeffrey RW, Goodier RJ, Payne JA, Moss SJ. Direct PKC-dependent phosphorylation regulates the cell surface stability and activity of the potassium chloride cotransporter, KCC2. 2007.

78. Buerli T, Pellegrino C, Baer K, Lardi-Studler B, Chudotvorova I, Fritschy J-M, et al. Efficient transfection of DNA or shRNA vectors into neurons using magnetofection. Nature protocols. 2007; 2(12):3090. https://doi.org/10.1038/nprot.2007.445 PMID: 18079708

79. Hartmann A-M, Pisella LI, Medina I, Nothwang HG. Molecular cloning and biochemical characterization of two cation chloride cotransporter subfamily members of Hydra vulgaris. PloS one. 2017; 12(6): e0179968. https://doi.org/10.1371/journal.pone.0179968 PMID: 28662098

80. Hartmann A-M, Wenz M, Mercado A, Störger C, Mount DB, Friauf E, et al. Differences in the large extracellular loop between the K+-Cl- cotransporters KCC2 and KCC4. The Journal of Biological Chemistry. 2010; 285(31):23994–4002. https://doi.org/10.1074/jbc.M110.144063 PMID: 20516068

81. Wisniewski JR. Quantitative Evaluation of Filter Aided Sample Preparation (FASP) and Multienzyme Digestion FASP Protocols. Analytical chemistry. 2016; 88(10):5438–43. https://doi.org/10.1021/acs.analchem.6b00859 PMID: 27119963

82. Wisniewski JR, Gaugaz FZ. Fast and sensitive total protein and Peptide assays for proteomic analysis. Analytical chemistry. 2015; 87(8):4110–6. https://doi.org/10.1021/ac504689z PMID: 25837572

83. Wisniewski JR, Nagaraj N, Zougman A, Gnad F, Mann M. Brain phosphoproteome obtained by a FASP-based method reveals plasma membrane protein topology. Journal of proteome research. 2010; 9(6):3280–9. https://doi.org/10.1021/pr1002214 PMID: 20415495

84. Wisniewski JR, Mann M. Consecutive proteolytic digestion in an enzyme reactor increases depth of proteomic and phosphoproteomic analysis. Analytical chemistry. 2012; 84(6):2631–7. https://doi.org/10.1021/ac300006b PMID: 22324799

85. Pinkse MW, Uitto PM, Hilhorst MJ, Ooms B, Heck AJ. Selective isolation at the femtomole level of phosphopeptides from proteolytic digests using 2D-NanoLC-ESI-MS/MS and titanium oxide precolumns. Analytical chemistry. 2004; 76(14):3935–43. https://doi.org/10.1021/ac0498617 PMID: 15253627

86. Lytle C, McManus T. Coordinate modulation of Na-K-2Cl cotransport and K-Cl cotransport by cell volume and chloride. American Journal of Physiol Cell Physiology. 2002; 283:1422–31.

87. Gagnon É, England R, Delpire E. Volume sensitivity of cation-Cl- cotransporter is modulated by the interaction of two kinases: Ste20-related proline-alanine-rich kinase and WNK4. American Journal of Physiol Cell Physiol. 2005a; 290:134–42.

88. Delpire E, Days E, Lewis LM, Mi D, Kim K, Lindsley CW, et al. Small-molecule screen identifies inhibitors of the neuronal K-Cl cotransporter KCC2. PNAS. 2009; 106(13):5383–8. https://doi.org/10.1073/pnas.0812756106 PMID: 19279215

89. Gillen CM, Brill S, Payne JA, Forbush B. Molecular Cloning and Functional Expression of the K-Cl Cotransporter from Rabbit, Rat and Human. The Journal of Biological Chemistry. 1996; 271:16237–44.

90. Culliford SJ, Ellory JC, Lang H-J, Englert H, Staines HM, Wilkins RJ. Specificity of classical and putative Cl-transport inhibitors on membrane transport pathways in human erythrocytes. Cellular Physiology and Biochemistry. 2003; 13(4):181–8. https://doi.org/10.1159/000072420 PMID: 12876375

91. Hornbeck PV, Kornhauser JM, Tkachev S, Zhang B, Skrzypek E, Murray B, et al. PhosphoSitePlus: a comprehensive resource for investigating the structure and function of experimentally determined post-translational modifications in man and mouse. Nucleic acids research. 2011; 40(D1):D261–D70.

92. Bergeron MJ, Gagnon KBE, Caron L, Isenring P. Identification of Key functional domains in the C Terminus of the K^+-Cl^- cotransporters. J Biol Chem. 2006; 281:15959–69. https://doi.org/10.1074/jbc.M600015200 PMID: 16595678

93. Vitari AC, Deak M, Morrice NA, Alessi DR. The WNK1 and WNK4 protein kinases that are mutated in Gordon's hypertension syndrome phosphorylate and activate SPAK and OSR1 protein kinases. Biochemical Journal. 2005; 391(1):17–24.

94. Zagórska A, Pozo-Guisado E, Boudeau J, Vitari AC, Rafiqi FH, Thastrup J, et al. Regulation of activity and localization of the WNK1 protein kinase by hyperosmotic stress. The Journal of cell biology. 2007; 176(1):89–100. https://doi.org/10.1083/jcb.200605093 PMID: 17190791

95. Uchida S, Sohara E, Rai T, Sasaki SJBotC. Regulation of with-no-lysine kinase signaling by Kelch-like proteins. 2014; 106(2):45–56.

96. Smith L, Smallwood N, Altman A, Liedtke CM. PKCδ acts upstream of SPAK in the activation of NKCC1 by hyperosmotic stress in human airway epithelial cells. Journal of Biological Chemistry. 2008; 283(32):22147–56. https://doi.org/10.1074/jbc.M801752200 PMID: 18550547

97. Del Castillo IC, Fedor-Chaiken M, Song JC, Starlinger V, Yoo J, Matlin KS, et al. Dynamic regulation of Na+-K+-2Cl− cotransporter surface expression by PKC-ε in Cl−-secretory epithelia. American Journal of Physiology-Cell Physiology. 2005; 289(5):C1332–C43. https://doi.org/10.1152/ajpcell.00580.2004 PMID: 16000638

98. Palmer R, Ridden J, Parker P. Identification of multiple, novel, protein kinase C-related gene products. FEBS letters. 1994; 356(1):5–8. https://doi.org/10.1016/0014-5793(94)01202-4 PMID: 7988719

99. Webb BL, Hirst SJ, Giembycz MA. Protein kinase C isoenzymes: a review of their structure, regulation and role in regulating airways smooth muscle tone and mitogenesis. British journal of pharmacology. 2000; 130(7):1433–52. https://doi.org/10.1038/sj.bjp.0703452 PMID: 10928943

100. Parker PJ, Murray-Rust J. PKC at a glance. Journal of cell science. 2004; 117(2):131–2.

101. Newton AC. Protein kinase C: structural and spatial regulation by phosphorylation, cofactors, and macromolecular interactions. Chemical reviews. 2001; 101(8):2353–64. https://doi.org/10.1021/cr0002801 PMID: 11749377

102. Flemmer AW, Gimenz I, Dowd BFX, Darman RB, Forbush B. Activation of the Na-K-Cl cotransporter NKCC1 detected with a Phospho-specific antibody. The Journal of Biological Chemistry. 2002; 277 (40):37551–8. https://doi.org/10.1074/jbc.M206294200 PMID: 12145305

103. Darman RB, Flemmer A, Forbush B. Modulation of ion transport by direct targeting of protein phosphatase type 1 tothe Na-K-Cl cotransporter. The Journal of Biological Chemistry. 2001; 276(37):34359–62. https://doi.org/10.1074/jbc.C100368200 PMID: 11466303

104. Lee HH, Deeb TZ, Walker JA, Davies PA, Moss SJJNn. NMDA receptor activity downregulates KCC2 resulting in depolarizing GABA A receptor–mediated currents. 2011; 14(6):736.

105. Salzer E, Santos-Valente E, Keller B, Warnatz K, Boztug KJJoci. Protein kinase C δ: a gatekeeper of immune homeostasis. 2016; 36(7):631–40.

106. Cheng N, He R, Tian J, Dinauer MC, Richard DYJTJoI. A critical role of protein kinase Cδ activation loop phosphorylation in formyl-methionyl-leucyl-phenylalanine-induced phosphorylation of p47phox and rapid activation of nicotinamide adenine dinucleotide phosphate oxidase. 2007; 179(11):7720–8.

107. Stempka L, Girod A, Müller H-J, Rincke G, Marks F, Gschwendt M, et al. Phosphorylation of Protein Kinase Cδ (PKCδ) at Threonine 505 is not a prerequisite for enzymatic activity expression of rat pkcδ and an alanine 505 mutant in bacteria in a functional form. 1997; 272(10):6805–11. https://doi.org/10.1074/jbc.272.10.6805 PMID: 9045715

108. Kahle KT, Deeb TZ, Puskarjov M, Silayeva L, Liang B, Kaila K, et al. Modulation of neuronal activity by phosphorylation of the K–Cl cotransporter KCC2. Trends in neurosciences. 2013; 36(12):726–37. https://doi.org/10.1016/j.tins.2013.08.006 PMID: 24139641

109. Kahle KT, Delpire E. Kinase-KCC2 coupling: Cl− rheostasis, disease susceptibility, therapeutic target. Journal of neurophysiology. 2015; 115(1):8–18. https://doi.org/10.1152/jn.00865.2015 PMID: 26510764

110. Kahle KT, Rinehart J, Lifton RP. Phosphoregulation of the Na–K–2Cl and K–Cl cotransporters by the WNK kinases. Biochimica et Biophysica Acta (BBA)-Molecular Basis of Disease. 2010; 1802 (12):1150–8.

111. Silayeva L, Deeb TZ, Hines RM, Kelley MR, Munoz MB, Lee HH, et al. KCC2 activity is critical in limiting the onset and severity of status epilepticus. Proceedings of the National Academy of Sciences. 2015; 112(11):3523–8.

112. Naik MU, Benedikz E, Hernandez I, Libien J, Hrabe J, Valsamis M, et al. Distribution of protein kinase Mζ and the complete protein kinase C isoform family in rat brain. Journal of Comparative Neurology. 2000; 426(2):243–58. https://doi.org/10.1002/1096-9861(20001016)426:2<243::aid-cne6>3.0.co;2-8 PMID: 10982466

113. Liu W, Heckman C. The sevenfold way of PKC regulation. Cellular signalling. 1998; 10(8):529–42. https://doi.org/10.1016/s0898-6568(98)00012-6 PMID: 9794251

114. Lauf PK, Adragna NC. K-Cl cotransport; properties and molecular mechanism. Cellular Physiology and Biochemistry. 2000; 10:341–54. https://doi.org/10.1159/000016357 PMID: 11125215

115. Yassin L, Radtke-Schuller S, Asraf H, Grothe B, Hershfinkel M, Forsythe ID, et al. Nitric oxide signaling modulates synaptic inhibition in the superior paraolivary nucleus (SPN) via cGMP-dependent suppression of KCC2. 2014; 8:65.

116. Chew TA, Orlando BJ, Zhang J, Latorraca NR, Wang A, Hollingsworth SA, et al. Structure and mechanism of the cation–chloride cotransporter NKCC1. 2019; 572(7770):488–92.

117. Liu S, Chang S, Han B, Xu L, Zhang M, Zhao C, et al. Cryo-EM structures of the human cation-chloride cotransporter KCC1. 2019; 366(6464):505–8.

118. Delpire E, Guo JJAJoP-CP. Cryo-EM structures of Dr NKCC1 and hKCC1: a new milestone in the physiology of cation-chloride cotransporters. 2020; 318(2):C225–C37.

119. Yang X, Wang Q, Cao EJNC. Structure of the human cation–chloride cotransporter NKCC1 determined by single-particle electron cryo-microscopy. 2020; 11(1):1–11.